The Journal of Immunology

RESEARCH ARTICLE | MARCH 27 2023

Dephosphorylation of T517 on Hemocyanin Is Required for Antibacterial Activity in *Penaeus vannamei* FREE

Qian Feng; ... et. al

J Immunol (2023) 210 (9): 1396–1407.
https://doi.org/10.4049/jimmunol.2200598

Dephosphorylation of T517 on Hemocyanin Is Required for Antibacterial Activity in *Penaeus vannamei*

Qian Feng,*,† Jude Juventus Aweya,‡ Yue-Qian Huang,* Pei Zhang,* Fan Wang,* De-Fu Yao,* Zhi-Hong Zheng,* En-Min Li,† and Yue-Ling Zhang*

Posttranslational modifications expand the functions of immune-related proteins, especially during infections. The respiratory glycoprotein, hemocyanin, has been implicated in many other functions, but the role of phosphorylation modification in its functional diversity is not fully understood. In this study, we show that *Penaeus vannamei* hemocyanin (*Pv*HMC) undergoes phosphorylation modification during bacterial infection. Dephosphorylation of *Pv*HMC mediated by *P. vannamei* protein phosphatase 2A catalytic increases its in vitro antibacterial activity, whereas phosphorylation by *P. vannamei* casein kinase 2 catalytic subunit α decreases its oxygen-carrying capacity and attenuates its in vitro antibacterial activity. Mechanistically, we show that Thr^{517} is a critical phosphorylation modification site on *Pv*HMC to modulate its functions, which when mutated attenuates the action of *P. vannamei* casein kinase 2 catalytic subunit α and *P. vannamei* protein phosphatase 2A catalytic, and hence abolishes the antibacterial activity of *Pv*HMC. Our results reveal that phosphorylation of *Pv*HMC modulates its antimicrobial functions in penaeid shrimp. ***The Journal of Immunology*****, 2023, 210: 1396–1407.**

Invertebrates defend and protect themselves against pathogens through humoral and cellular innate immune mechanisms (1, 2). The cellular innate immune response of invertebrates employs several mechanisms, including phagocytosis and apoptosis by immunocytes, such as hemocytes (3), whereas the humoral immune responses involve nonspecific enzymes or factors in hemolymph, including phenoloxidase, lectins, and antimicrobial peptides (AMPs), among others, which clear pathogens by direct or indirect killing (4–6).

To increase their ability to mount broad-spectrum immune responses, invertebrates encode many factors and genes with high molecular diversity. In the fruit fly, *Drosophila*, depletion of the Down syndrome cell adhesion molecule (Dscam), a member of the Ig superfamily that undergoes multiple alternative splicing to generate numerous gene products, impairs the ability of hemocytes to phagocytose *Escherichia coli* (7). Similarly, bacteria-specific Dscam isoforms (e.g., *Es*Dscam$_{(4.24,6.19)}$ and *Es*Dscam$_{(4.12,6.20)}$) are produced in Chinese mitten crab (*Eriocheir sinensis*) via alternative splicing (8). In *Drosophila* and the freshwater snail (*Biomphalaria*), *v*ariants of the fibrinogen-related proteins (FREPs), that is, FREP2, FREP3, and FREP4, are involved in the innate immune response, such as pathogen agglutination, bacterial clearance, and antiparasite defense (9–11). In penaeid shrimp, C-type lectins are important pathogen recognition molecules with high diversity in domain architecture, sugar substrates, tissue distribution, pathogen-induced expression patterns, and immune functions (12). Many naturally occurring AMPs in penaeid shrimp have also been shown to possess genetic variations that diversify their antimicrobial activities. For instance, crustinPm4 in *Penaeus monodon* has both antibacterial and antiviral activities (13), whereas CrustinPm7 displays only antibacterial activity (14). Several penaeidin isoforms in *P. vannamei*, generated by polymorphism within the proline and cysteine-rich domains, possess different antimicrobial activities, that is, antibacterial, antifungal, and antiviral (15, 16).

The regulation of eukaryotic proteins generally takes place at the DNA, mRNA, protein, and posttranslational modification (PTM) levels to modulate their functions and expression (17). For most proteins, PTM is critical for the regulation of their

*Institute of Marine Sciences and Guangdong Provincial Key Laboratory of Marine Biotechnology, Shantou University, Shantou, China; †The Key Laboratory of Molecular Biology for High Cancer Incidence Coastal Chaoshan Area, Medical College, Shantou University, Shantou, China; and ‡College of Ocean Food and Biological Engineering, Fujian Provincial Key Laboratory of Food Microbiology and Enzyme Engineering, Jimei University, Xiamen, Fujian, China

ORCIDs: 0000-0002-6059-6956 (F.W.); 0000-0002-0510-8307 (Y.-L.Z.).

Received for publication August 16, 2022. Accepted for publication December 18, 2022.

This work was supported by the National Natural Science Foundation of China Grants 31872596 and U22A20536, 2020 Li Ka Shing Foundation Cross-Disciplinary Research Grant 2020LKSFG01E), and by Natural Science Foundation of Guangdong Province Grant 2214050002866.

Conceptualization, Y.-L.Z. and E.-M.L.; funding acquisition, Y.-L.Z.; investigation, Q.F., Y.-Q.H., and P.Z.; resources, F.W., D.-F.Y., and Z.-H.Z.; supervision, Y.-L.Z., E.-M.L., J.J.A., and D.F.Y.; writing—original draft, Q.F. and J.J.A.; writing—review and editing, Q.F., J.J.A., Y.-L.Z., and E.-M.L. All authors have read and agreed to the published version of the manuscript.

The mass spectrometry proteomics data presented in this article have been submitted to the PRIDE database under accession numbers PXD032927 and PXD033605.

Address correspondence and reprint requests to Prof. Yue-Ling Zhang or Prof. En-Min Li, Institute of Marine Sciences, College of Science, Shantou University, Daxue Road 243, Shantou, Guangdong 515063, China (Y.-L.Z.) or Shantou University Medical College, No. 22, Xinling Road, Shantou, Guangdong 515041, China (E.-M.L.). E-mail addresses: zhangyl@stu.edu.cn (Y.-L.Z.) or nmli@stu.edu.cn (E.-M.L.)

The online version of this article contains supplemental material.

Abbreviations used in this article: AMP, antimicrobial peptide; Co-IP, coimmunoprecipitation; d*Pv*HMC, dephosphorylated PvHMC; d*Pv*HMCc, d*Pv*HMC, where "c" represents *Pv*CK2α knockdown shrimp; d*Pv*HMCp, d*Pv*HMC, where "p" represents treated in vitro with recombinant GST-*Pv*PP2AC; Dscam, Down syndrome cell adhesion molecule; HEK293T, human embryonic kidney 293T; IMD, immune deficiency; LB, Luria-Bertani; LTA, lipoteichoic acid; MS, mass spectrometry; PGN, peptidoglycan; p*Pv*HMCc, phosphorylated samples of d*Pv*HMCc treated in vitro with *Hs*CK2; p*Pv*HMCn, phosphorylated *Pv*HMC samples from control siNon-injected shrimp; PTM, posttranslational modification; *Pv*CK2α, *Penaeus vannamei* casein kinase 2 catalytic subunit α; PVDF, polyvinylidene difluoride; *Pv*HMC, *Penaeus vannamei* hemocyanin; *Pv*HMCL, large molecular mass subunit of *Pv*HMC; *Pv*HMCS, small molecular mass subunit of *Pv*HMC; *Pv*PP2AC, *Penaeus vannamei* protein phosphatase 2A catalytic; qPCR, quantitative PCR; RNAi, RNA interference; S2, Schneider 2; siNon, scrambled control siRNA; siRNA, small interfering RNA; sNASP, somatic nuclear autoantigenic sperm protein.

physical and chemical properties, folding, conformation, stability, activity, and biological functions (18, 19), and modulation of immunity (20). In *Drosophila*, ubiquitylation of the caspase-8 ortholog, death-related ced-3/Nedd2-like protein (DREDD), is required for the full processing of immune deficiency (IMD), NF-κB/Relish, and expression of AMP genes in response to bacteria (Gram-negative) infection (21). Similarly, the deacetylation of histone proteins in *Drosophila* activates intestinal innate immunity via regulation of IMD signaling (22), whereas trimethylation of histone H3 (on lysine 4) enhances gut innate immunity to help maintain bacteria and metabolic homeostasis through Toll/IMD signaling regulation (23). In crustaceans, various histone proteins undergo PTM to enhance their antimicrobial activity, including the acetylation of histones H2B and H4, phosphorylation of histones H2A and H4, and methylation of histone H4 in penaeid shrimp (24), whereas the phosphorylation of focal adhesion kinase (FAK) in *Marsupenaeus japonicus* promotes an antiviral response during white spot syndrome virus infection (25). Additionally, Dock protein promotes the phosphorylation of ERK in *E. sinensis* to modulate the phosphorylation and translocation of Dorsal to induce AMP expression (26). We also recently reported that the acetylation/deacetylation modification of *P. vannamei* hemocyanin (*Pv*HMC) plays a vital role in its antimicrobial activity. We revealed that the deacetylation of *Pv*HMC enhances its antibacterial activity by increasing its binding with LPS and destruction of Gram-negative bacteria, whereas its acetylation, especially on residues K481 and K484, attenuates its binding with LPS and therefore its antibacterial activity (27).

Hemocyanin is a copper-containing respiratory protein that constitutes ~90% of plasma proteins in arthropods and mollusks (28). Arthropodan hemocyanin is composed of single or multiple hexamers, with each subunit having three domains, whereas molluskan hemocyanin is a cylindrical decamer or polymer of ~350 or 400 kDa (29). Although hemocyanin is primarily involved in the transport of molecular oxygen (30), numerous studies have implicated hemocyanin in many immune-related activities, including phenoloxidase (31), antiviral (32), antimicrobial (33), agglutinative (34), hemolytic activity (35), antitumor (36), degradation into antimicrobial and antiviral peptides (37, 38), and interaction with immune-related cellular signaling pathway molecules (39), among others. These multiple functions of hemocyanin could be due to molecular diversity, variant forms, and PTMs. For instance, C- and N-terminal SNPs in *Pv*HMC (40, 41) and splicing variants play a key role in the antimicrobial activity of *Pv*HMC (42). Similarly, *N*-glycosylation of hemocyanin in mollusks *Rapana venosa*, *Helix lucorum*, and *Megathura crenulata* (32, 43) and penaeid shrimp (*P. vannamei*) affect its functions (44). Moreover, the C-terminal of *Pv*HMC interacts with and activates the ERK1/2 signaling pathway during Taura syndrome virus (TSV) infection (45), while our recent study revealed that *Pv*HMC interacts via its armadillo (ARM) repeat domain with *Pv*MKK4 to modulate the p38 MAPK signaling pathway (39), highlighting the significance of phosphorylation in the antimicrobial activity of *Pv*HMC. Thus, given the importance of phosphorylation modification in the modulation of protein function, especially immune-related proteins (20), we explored mechanistically how phosphorylation of *Pv*HMC affects its antimicrobial activity in *P. vannamei*. In this study, we reveal that *Pv*HMC undergoes dephosphorylation mediated by the casein kinase 2 catalytic subunit α (*Pv*CK2α) and protein phosphatase 2A catalytic (*Pv*PP2AC) to enhance its antibacterial activity. Threonine 517 on the large molecular mass subunit of *Pv*HMC (*Pv*HMCL) was found to be the crucial amino acid residue that upon phosphorylation or dephosphorylation alters the antimicrobial activity of *Pv*HMC.

Materials and Methods

Experimental animals

Pacific white shrimp, *P. vannamei*, weighting 5–8 g, obtained from Shantou Huaxun Aquatic Product Corporation (Shantou, China), were cultured in air-circulating laboratory tanks containing artificial seawater (salinity of 10 ppm and temperature 25°C) for 2 d before experiments. During the laboratory acclimation period, shrimp were fed a commercial diet (35% protein) once daily. All animal experiments were carried out in accordance with the guidelines and approval of the Animal Research and Ethics Committees of Shantou University (Shantou, China).

Reagents and plasmids

To express GST-tagged proteins in prokaryotic cells, DNA sequences were amplified by PCR before being subcloned into the pGEX-6p-1 vector (Solarbio, Beijing, China). The *Pv*CK2α (GenBank: KY038483.1) and *Pv*PP2AC (GenBank: XP_027227758.1) DNA sequences were PCR amplified and subcloned into the pGEX-6p-1 vector at the BamHI and SmaI sites to generate the pGEX-6P-1-*Pv*CK2α and pGEX-6p-1-*Pv*PP2AC plasmids. For eukaryotic expression, the open reading frame of the small molecular mass subunit of the *Pv*HMC (*Pv*HMCS) gene (UniProtKB: A0A1Y0DT76) and the *P. vannamei Pv*HMCL gene (UniProtKB: A0A059TEW9) with Flag-tag at C-terminal were subcloned into the pIZ/V5-His vector (Life Technology, Carlsbad, CA) at the BamHI and XhoI sites to generate the pIZ-*Pv*HMCS-EGFP-Flag and pIZ-*Pv*HMCL-EGFP-Flag plasmids. As control, pIZ-EGFP-Flag plasmid was also constructed. Similarly, the open reading frame sequence of *Pv*HMCL was subcloned into the pcDNA3.1$^+$ vector (Thermo Fisher Scientific, Waltham, MA) at the XhoI restriction sites using the ClonExpress II one step cloning kit (Vazyme, Nanjing, China) to generate the *Pv*HMCL-Flag plasmid with a Flag-tag at the C-terminal. Phosphorylation sites mutant plasmids of *Pv*HMCL-Flag (T517A and T517E) were constructed using the Fast mutagenesis system kit (TransGen Biotech, Beijing, China). The oligonucleotides used for plasmid construction are listed in Supplemental Table I.

Cell culture

Drosophila Schneider 2 (S2) cells (a gift from Dr. Haoyang Li of the School of Marine Science, Sun Yat-sen University, China) were cultured at 27°C in Schneider's *Drosophila* medium (Invitrogen, Carlsbad, CA) supplemented with 10% FBS (Life Technologies, Carlsbad, CA). Human embryonic kidney 293T (HEK293T) cells, which were a kind gift from Prof. En Min Li of Shantou University Medical College (Shantou University, Shantou, China) were grown in DMEM (Thermo Fisher Scientific, Waltham, MA) supplemented with 10% FBS and 1% penicillin/streptomycin (Life Technologies, Carlsbad, CA) and maintained at 37°C in a 5% CO_2 humidified incubator.

SDS-PAGE and Western blot

Protein samples were mixed with 5× loading buffer (42 mM Tris-HCl, containing 100 ml/l glycerol, 23 g/l SDS, 50 g/l 2-ME, and 0.02 g/l bromophenol blue) before being boiled for 6 min. Next, samples were separated on 10% SDS-PAGE gels and transferred onto polyvinylidene difluoride (PVDF) membranes (Millipore, Billerica, MA) using the Mini Trans-Blot electrophoretic transfer cell (Bio-Rad, Hercules, CA). The membranes were then blocked for 2 h at room temperature in 5% skimmed milk dissolved in TBST buffer (20 mM Tris, 150 mM NaCl, 0.1% Tween 20 [pH 7.6]), followed by overnight incubation at 4°C or 1 h at room temperature with primary Abs. After being washed three times with TBST buffer (15 min each time), membranes were incubated for 1 h at room temperature with secondary Abs. Membranes were then washed three times with TBST buffer (15 min each time) and the signals were detected by chemiluminescence using ECL-detecting reagent, and images were captured using the GE Amersham Imager 600 imaging system (GE Healthcare, Boston, MA).

ELISA assay

The binding of phosphorylated *Pv*HMC with LPS or peptidoglycan (PGN) was determined by ELISA. Briefly, 100 μl/well of various concentrations of LPS (Sigma-Aldrich, St. Louis, MO) or PGN (Sigma-Aldrich, St. Louis, MO) (0, 25, 50, and 100 μg/ml) were added to 96-well plates and incubated overnight at 4°C. After plates were blocked for 2 h with 200 μl/well 3% BSA in PBS (0.15 M [pH 7.4]) at room temperature and washed four times with PBS (200 μl/well), 100 μl/well purified *Pv*HMC diluted with PBS (0.15 M [pH 7.4]) containing 0.1 mg/ml BSA (50 μg/ml) was added before being incubated at room temperature for 3 h. Next, plates were washed four times with PBS (200 μl/well) and incubated for 1 h with 100 μl of primary Ab at room temperature. After being washed four times with PBS (0.15 M [pH 7.4]), plates were incubated for 45 min with 100 μl of peroxidase-conjugated secondary Ab at room temperature. The plates were then

washed and developed with 100 μl of 3,3′,5,5′- tetramethylbenzidine (Beyotime, Shanghai, China). The reaction was stopped with 2 M H_2SO_4, and absorbance was read at 450 nm. Triplicate samples were analyzed per each treatment and repeated at least three independent times.

Abs used

For Western blot analysis, the primary Abs used include rabbit anti-CK2α Ab (Thermo Fisher Scientific, Waltham, MA, 1:1000), rabbit anti-PP2AC Ab (Beyotime, Shanghai, China, 1:1000), mouse anti-tubulin Ab (Sigma-Aldrich, St. Louis, MO, 1:3000), mouse anti-GST Ab (TransGen Biotech, Beijing, China, 1:3000), mouse anti-Flag Ab (TransGen Biotech, Beijing, China, 1:3000), rabbit anti-p-Ser/p-Thr/p-Try Abs (Immunechem, Burnaby, BC, Canada, 1:3000), and in-house prepared rabbit anti-shrimp hemocyanin antisera (46) used at 1:5000 dilution. In the ELISA assay, rabbit anti-*Pv*HMC Ab (made in-house) was used at 1:1000 dilution. The rabbit polyclonal Ab to *Pv*HMCL-p-Thr^{517}, which was commissioned by a commercial company (DIA-AN, Wuhan, China) was generated by immunization of rabbits with the peptide c(KLH)NGIKF-pT-FDEGR (where c(KLH) indicates keyhole limpet hemocyanin fused through cysteine, and pT indicates phosphorylated threonine). The secondary Abs were goat anti-rabbit IgG-HRP (Thermo Fisher Scientific, Waltham, MA, 1:5000) and goat anti-mouse IgG-HRP (Thermo Fisher Scientific, Waltham, MA, 1:5000) for Western blot analysis. Peroxidase-conjugated goat anti-rabbit IgG Ab (1:2000) was the secondary Ab used in the ELISA assay.

Immune challenge and cell lysis

For bacteria challenge experiments, each shrimp was injected between the third and fourth segments of the muscle with 0.5×10^6 CFU/g of *Vibrio parahaemolyticus*, *Streptococcus iniae*, LPS (0.5 mg/ml), and lipoteichoic acid (LTA) (Sigma-Aldrich, St. Louis, MO, 0.5 mg/ml) or with an equal volume of sterile PBS (0.01 M [pH 7.4]) as control. At different time points (0, 6, 12, 24, 36, 48, 72, and 96 h) hemolymph was withdrawn from seven shrimp per group into an equal volume of precooled anticoagulant (336 mM NaCl, 115 mM glucose, 27 mM sodium citrate, 9 mM EDTA-Na_2·$2H_2O$ [pH 7.0]) as previously described (47). Next, hemolymph was centrifuged at 800 × *g* (15 min at 4°C) to collect hemocytes and plasma. Hemocytes were washed thoroughly with PBS (0.01 M [pH 7.4]), lysed with lysis buffer (25 mM HEPES, 150 mM NaCl, 1% Triton X-100, 1 mM EDTA-Na_2·$2H_2O$ [pH 7.4]) plus protease inhibitor (PMSF, Beyotime, Shanghai, China) for 30 min before being centrifuged at 20,000 × *g* (15 min at 4°C) to collect the supernatant. The total protein concentration levels of cell lysates and plasma were determined by a modified Bradford assay (GenStar, Beijing, China) using BSA as a standard. Samples were used immediately for the next experiment or stored in aliquots at −40°C for later use.

RNA interference and inhibitor treatment

The small interfering RNA (siRNA) targeting *Pv*CK2α (GenBank: KY038483.1), *Pv*PP2AC (GenBank: XP_027227758.1), and scrambled control siRNA (siNon) were designed (see Supplemental Table I) and chemically synthesized by a commercial company (GenePharma, Suzhou, China). To perform the RNA interference (RNAi) experiments, shrimp were divided into three groups (20 each). The experimental group shrimps were each injected with 100 μl (0.5 μg/g shrimp) of the respective siRNA, whereas control group shrimps were injected with an equivalent amount of siNon. To inhibit the expression of CK2α or PP2AC, shrimp (10 each) were also injected with CX-4945 (MedChemExpress, Monmouth Junction, NJ), CK2α inhibitor, or okadaic acid (Beyotime, Shanghai, China), a PP2AC inhibitor. Briefly, shrimps were injected with 100 μl of CX-4945 (100 μg/ml in 0.01 M PBS) or 100 μl of Okadaic acid (10 μg/ml in 0.01 M PBS [pH 7.4]), whereas control group shrimp were injected with an equivalent volume of vehicle (0.01 M PBS [pH 7.4]). Hemolymph was withdrawn at different time points from five randomly selected shrimp per group for analysis of *Pv*CK2α and *Pv*PP2AC expression and *Pv*HMC phosphorylation level.

Total RNA extraction, cDNA synthesis, and real-time quantitative PCR analysis

Total RNA was extracted from hepatopancreas and hemocyte samples using TRIzol reagent (Invitrogen, Carlsbad, CA) following the protocol of the manufacturer. The RNA concentration was determined with a NanoDrop 2000 spectrophotometer (NanoDrop Technologies, Wilmington, DE), and RNA quality was ascertained using the A260/280 ratio (≥2) and on 1% agarose gel electrophoresis. Only good quality RNA samples were used for further analysis. First-strand cDNA synthesis was carried out with 1.0 μg of total RNA using a one-step genomic DNA removal and cDNA synthesis supermix kit (TransGen Biotech, Beijing, China). In the real-time quantitative PCR (qPCR), primers targeting *Pv*CK2α, *Pv*PP2AC, and the elongation factor 1 α gene of *P. vannamei* (*Pv*EF1α) were designed using Primer Premier 5 software (Supplemental Table I). The qPCR reactions were carried out on the qTOWER^{3}G real-time qPCR system (Analytik Jena, Jena, Germany) with the following program: one cycle at 95°C for 10 min, 45 cycles of 95°C for 15 s, and 60°C for 30 s. The data were analyzed by the $2^{-\Delta\Delta Ct}$ method (48) with the *Pv*EF1α gene used as the internal control.

Protein expression and purification

Shrimp plasma hemocyanin was purified as previously described (49). Briefly, hemolymph from *P. vannamei* was centrifuged (500 × *g*, 10 min at 4°C) using Vivaspin 2 centrifuge filter units (Sartorius, Gottingen, Germany) followed by gel filtration chromatography (Superose 6 Increase 10/300 GL, GE Healthcare, Boston, MA) on an ÄKTA pure system (GE Healthcare, Boston, MA).

For eukaryotic expression of the proteins *Pv*HMCL-Flag, *Pv*HMCLT517A-Flag, and *Pv*HMCLT517E-Flag, HEK293T cells were transfected with the plasmids pcDNA3.1-*Pv*HMCL, pcDNA3.1-*Pv*HMCLT517A-Flag, and pcDNA3.1-*Pv*HMCLT517E-Flag, respectively, before being cultured in DMEM (Thermo Fisher Scientific, Waltham, MA) with 10% FBS (Life Technologies, Carlsbad, MA) at 37°C. After 48 h, cells were harvested and lysed for 30 min in lysis buffer (25 mM HEPES, 150 mM NaCl, 1% Triton X-100, 1 mM EDTA-Na_2·$2H_2O$ [pH 7.4]) plus protease inhibitor mixture (MedChemExpress, Monmouth Junction, NJ) and PMSF before being centrifuged at 20,000 × *g* (15 min at 4°C) to collect the supernatant. Cell lysates were incubated with anti-Flag magnetic beads (MedChemExpress, Monmouth Junction, NJ) at 4°C for 4 h before being centrifuged at 1000 × *g* (5 min at 4°C). After discarding the supernatant, beads were washed five times with wash buffer TBST (50 mM Tris-HCl, 150 mM NaCl, 0.5% Tween 20 [pH 7.4]) and then incubated with elution buffer (1 mg/ml 3× Flag peptide, 50 mM Tris, 0.15 M NaCl [pH 7.4]). Next, samples were dialyzed with 0.01 M PBS in 30-kDa filter devices (Millipore, Billerica, MA) followed by centrifugation 10 times at 12,000 × *g* (2 min at 4°C). The purified proteins were collected and stored at −40°C for later use.

For prokaryotic expression, *E. coli* strain BL21 (DE3) (TransGen Biotech, Beijing, China) transformed with plasmids expressing GST-*Pv*CK2α, GST-*Pv*PP2AC, and GST proteins were grown at 37°C in Luria-Bertani (LB) medium with 50 mg/l ampicillin until an OD_{600} of 0.6 was reached before being induced with 1 mM isopropyl β-D-thiogalactoside (GenStar, Beijing, China) at 16°C and then cultured to an OD_{600} of 1.2. Next, cells were harvested by centrifugation (5000 × *g*, 20 min at 4°C) and lysed by sonication in fresh lysis buffer without detergent (8 mM Na_2HPO_4, 137 mM NaCl, 2 mM NaH_2PO_4, protease inhibitor mixture [MedChemExpress, Monmouth Junction, NJ], and PhosSTOP [Roche, Basel, Switzerland]). After sonication for 30 min, Triton X-100 was added to a final concentration of 0.5% before being centrifuged. The GST-*Pv*CK2α, GST-*Pv*PP2AC, and GST proteins were purified by glutathione Sepharose 4B (GE Healthcare, Boston, MA). Briefly, the clear supernatant containing soluble proteins (GST-*Pv*CK2α, GST-*Pv*PP2AC, and GST) were incubated with glutathione Sepharose 4B beads at 4°C for 1 h, followed by washing 10 times with 0.01 M PBS (with 0.5% Triton X-100 [pH 7.4]) to remove unconjugated proteins. The beads conjugated to GST-*Pv*CK2α, GST-*Pv*PP2AC, and GST were analyzed by immunoblotting or stored at −40°C for later use.

Pulldown and coimmunoprecipitation assay

In the GST pulldown assays, purified hemocyanin (see *Protein expression and purification*) was incubated with GST-*Pv*CK2α, GST-*Pv*PP2AC, or GST at 4°C for 0.5 h. Next, samples were washed 10 times with 0.01 M PBS (plus 0.5% Triton X-100 [pH 7.4]) before being analyzed by SDS-PAGE and Western blot as described under *SDS-PAGE and Western blot*. The coimmunoprecipitation (Co-IP) analysis was carried out as previously described (39). Briefly, *Drosophila* S2 cells were transfected with the plasmids pIZ-*Pv*HMCS-EGFP-Flag, pIZ-*Pv*HMCL-EGFP-Flag, pIZ-*Pv*PP2AC-V5, and pIZ-EGFP-Flag (control). At 48 h posttransfection, cells were harvested and washed three times with ice-cold PBS (0.01 M [pH 7.4]), followed by lysis in immunoprecipitation lysis buffer (25 mM HEPES, 150 mM NaCl, 1 mM EDTA-Na_2·$2H_2O$, 1% Triton X-100 [pH 7.4]) with protease inhibitor mixture (MedChemExpress, Monmouth Junction, NJ). Next, cell lysates were incubated at 4°C for 4 h with anti-Flag Ab magical beads (MedChemExpress, Monmouth Junction, NJ) followed by washing 10 times with freshly prepared lysis buffer and the precipitated proteins mixed with 5× loading buffer. Samples were then separated by SDS-PAGE and transferred onto PVDF membranes followed by Western blot analysis as described under *SDS-PAGE and Western blot*.

Immunoprecipitation

Immunoprecipitation was carried out as previously described (50). Briefly, the shrimp hemocytes and plasma from *Immune challenge and cell lysis* were harvested and washed five times with cold anticoagulant. The hemocytes followed by lysis in Western and immunoprecipitation lysis buffer (Beyotime, Shanghai, China) with protease inhibitor mixture (MedChemExpress, Monmouth Junction, NJ). Next, cell lysates were centrifuged at 20,000 × *g* for 15 min at 4°C. The plasma was diluted with PBS. Protein concentrations were determined using a Pierce bicinchoninic acid protein assay kit (GenStar, Beijing, China) and adjusted to the final volume of 600 μl at a concentration of 1 mg/ml using lysis buffer. Samples of 30 μl of supernatants mixed with 10 μl of 4× loading buffer were boiled for 5 min at 100°C as total input. The other supernatants were incubated with 2 μg of rabbit anti-shrimp hemocyanin Ab or rabbit anti-*Pv*HMCL-p-Thr^{517} Ab overnight at 4°C and then with 20 μl of protein A/G magnetic beads (MedChemExpress, Monmouth Junction, NJ) for 1 h. The beads were washed five times with lysis buffer and boiled in 20 μl of 2× loading buffer for 10 min at 100°C. Samples were then separated by SDS-PAGE and transferred onto PVDF membranes followed by Western blot analysis as described under *SDS-PAGE and Western blot*.

In vitro phosphorylation and dephosphorylation

To perform in vitro phosphorylation of hemocyanin, dephosphorylated *Pv*HMC (1 mg) was incubated at 30°C for 6 h with commercial human CK2, *Hs*CK2 (New England Biolabs, Ipswich, MA), 10× NEB buffer (50 mM Tris-HCl,10 mM $MgCl_2$, 0.1 mM EDTA, 2 mM DTT, 0.01% Brij 35 [pH 7.5]), 0.5 μl of *Hs*CK2, and 10 μl of ATP (NEB, Beijing, China). For in vitro dephosphorylation of hemocyanin, *Pv*HMC (600 μg) was incubated at 37°C for 4 h with recombinant GST-PP2A (see *Protein expression and purification*), 15 μl of 10× CutSmart buffer (0.1 M Tris-HCl, 1 M $MgCl_2$, 50 mM EDTA, 1 M DTT [pH 7.5]), and 3 μg of GST-PP2A beads. Next, one-half of the samples were mixed with an equal volume of protein loading buffer before being analyzed by SDS-PAGE and Western blot. The other half of the samples were used immediately for the next experiment or stored at −40°C for later use.

Mass spectrometry

To identify the phosphorylation sites on *Pv*HMC, *Pv*HMC samples (p*Pv*HMCn, phosphorylated *Pv*HMC samples from control siNon-injected shrimp; d*Pv*HMCc, dephosphorylated *Pv*HMC [d*Pv*HMC], where "c" represents *Pv*CK2α knockdown shrimp; and p*Pv*HMCc, phosphorylated samples of d*Pv*HMCc treated in vitro with *Hs*CK2) were separated by SDS-PAGE followed by mass spectrometry (MS). Briefly, the phosphorylated *Pv*HMC samples were prepared and purified as described under *RNA interference and inhibitor treatment* and *Protein expression and purification*, before being boiled with 5× loading buffer, separated on SDS-PAGE, and stained with Coomassie Blue (GenStar, Beijing, China). Next, excised protein bands were destained, reduced, and alkylated before being digested with trypsin (Promega, Madison, WI). Phosphorylated *Pv*HMC peptides were collected by Si-TiO_2 MagBeads (PuriMag Biotech, Xiamen, China) following the manufacturer's instructions before being analyzed by liquid chromatography–MS/MS, and the phosphorylated peptides were analyzed on an EASY-nLC 1000 system (Thermo Fisher Scientific, Waltham, MA) coupled to an LTQ Orbitrap Elite mass spectrometer (Thermo Fisher Scientific, Waltham, MA) equipped with a PicoChip source (New Objective, Littleton, MA). The sample parameters of the mass spectrometry have been described previously (51). The acquired MS/MS data were analyzed using Proteome Discoverer 2.2 software (Thermo Fisher Scientific, Waltham, MA) based on the UniProtKB *P. vannamei* database (https://www.uniprot.org).

Oxygen-carrying capacity assay

The oxygen-carrying capacity of *Pv*HMC samples (collected as described under *Protein expression and purification*) was determined using an improved polarographic fluorometric method, which employs an enzymatic method to analyze changes in dissolved oxygen concentration (52). Briefly, the optimal excitation wavelengths (285 nm) and emission wavelengths (330 nm) of *Pv*HMC were determined by three-dimensional scanning fluorescence spectrophotometry (Tecan Spark; Tecan, Männedorf, Switzerland) (Supplemental Fig. 2A). Next, purified *Pv*HMC samples (described under *RNA interference and inhibitor treatment* and *Total RNA extraction, cDNA synthesis, and real-time quantitative PCR analysis*) were diluted in an equal volume of buffer (100 mM Tris-HCl [pH 7.8]/5 mM $MgCl_2$/5 mM $CaCl_2$), and the final concentration was adjusted to 200 μg/ml, followed by the addition of 10 U/ml glucose oxidase and 1000 U/ml catalase to each sample before being aliquoted into 2-ml samples. Deionized H_2O, H_2O_2 (0.3%), and glucose solution (1 M) were then added to each well (see Supplemental Fig. 2B) followed by incubation at room temperature for 5 min and detection of the oxygen-binding curves in terms of fluorescence intensity using a microplate reader (Tecan Spark; Tecan, Männedorf, Switzerland). The dissolved oxygen concentration was determined using an Oxygraph (Hansatech, Norfolk, U.K.). The oxygen-binding capacity of *Pv*HMC is represented by increased fluorescence intensity in the fixed dissolved oxygen concentration range.

In vitro Pv*HMCs antibacterial and bacteria binding assay*

The antibacterial activity of *Pv*HMCs was determined using bacterial inhibition and bacterial agglutination assays (53). For the bacterial inhibition assay, purified *Pv*HMC was filter (0.22 μm) sterilized, whereas Gram-negative bacteria (*V. parahaemolyticus*, *Vibrio alginolyticus*, *Photobacterium damselae*, and *E. coli* K12) and Gram-positive bacteria (*S. iniae* and *Staphylococcus aureus*) were grown overnight in LB medium. Bacteria were collected by centrifugation, washed three times with 0.85% NaCl, and then resuspended with 50 mM Tris-HCl (pH 7.2) to a density of 10^3 CFU/ml. Sterile *Pv*HMCs or 0.01 M (pH 7.4) PBS (control) were mixed separately with each bacteria suspension before being incubated at room temperature for 30 min. Next, 50 μl of incomplete nutrient medium (0.04% Bacto tryptone, 0.02% yeast extract, 0.75% NaCl, 50 mM $CaCl_2$, 50 mM Tris-HCl [pH 7.2]) was added to each sample and incubated for another 1.5 h before being spread on LB Petri dishes and incubated at 37°C for 12 h. The numbers of bacteria colonies were counted as a measure of the CFU, whereas the bacteria inhibition rate was calculated as follows: Inhibition rate = [(clones in negative control − clones in the experimental group)/clones in negative control] × 100%. All samples was prepared and analyzed in triplicates for at least three independent samples.

A bacterial agglutination assay was performed as previously described. Briefly, Gram-negative (*V. parahaemolyticus*, *V. alginolyticus*, *P. damselae,* and *E. coli* K12) and Gram-positive (*S. iniae* and *S. aureus*) bacteria were cultured to mid-logarithmic phase in LB medium before being harvested by centrifugation at 12,000 × *g* for 1 min. After washing bacteria pellets three times with TBS, TBS (20 mM Tris-HCl, 150 mM NaCl [pH 7.4]), and diluted to 10^8 CFU/ml in TBS-Ca^{2+} buffer (0.05 M Tris, 0.75% NaCl, 0.05 M $CaCl_2$), bacteria suspensions were mixed in an equal volume (20 μl) with sterile *Pv*HMC diluted 2-fold in TBS-Ca^{2+} buffer, before being incubated at 37°C for 30 min. Bacteria agglutination was observed under a light microscope (Mshot; Guangzhou Micro-shot Technology, Guangzhou, China) and scored as positive (+) or negative (−) compared with control samples treated with only TBS-Ca^{2+} buffer. All samples were analyzed in triplicates and repeated at least three independent times. The agglutinative titer was defined as the highest dilution of the test samples when the agglutination appeared.

The bacteria binding ability of phosphorylated *Pv*HMC with Gram-negative (*V. parahaemolyticus*, *V. alginolyticus*, *P. damselae*, and *E. coli* K12) and Gram-positive (*S. iniae* and *S. aureus*) bacteria was analyzed as previously described (54). Briefly, 200 μl of *Pv*HMC or PBS (0.01 M [pH 7.4]) was incubated separately with mid-logarithmic phase bacteria (2.0×10^8 CFU/ml) at 37°C for 0.5 h. Next, bacteria cells were harvested by centrifugation and washed six times with PBS (0.01 M [pH 7.4]), followed by analysis of bacteria-*Pv*HMC by SDS-PAGE and Western blot using anti-*Pv*HMC Ab. Triplicate experiments were analyzed per sample and repeated at least three independent times.

Data availability

The mass spectrometry proteomics data of hemocyanin phosphorylation sites have been deposited to the ProteomeXchange Consortium via the PRIDE database with the dataset identifier PXD032927 (https://www.ebi.ac.uk/pride/archive/projects/PXD032927), and those of the protein–protein interaction of hemocyanin with other proteins have the dataset identifier PXD033605 (https://www.ebi.ac.uk/pride/archive/projects/PXD033605).

Results

Hemocyanin undergoes bacterial-induced phosphorylation

When shrimp were challenged with Gram-negative bacteria (*V. parahaemolyticus*), the p-Ser levels of *Pv*HMC in plasma increased at 6 h followed by an increase from 12 to 72 h. In contrast, the p-Thr and p-Tyr levels of *Pv*HMC in plasma decreased followed by an increase between 6 and 72 h (Fig. 1B, Supplemental Fig. 1A). In response to challenge by Gram-positive bacteria (*S. iniae*), the p-Ser, p-Thr, and p-Tyr levels of *Pv*HMC decreased followed by an increase from 6 to 72 h (Fig. 1C). Similarly, the

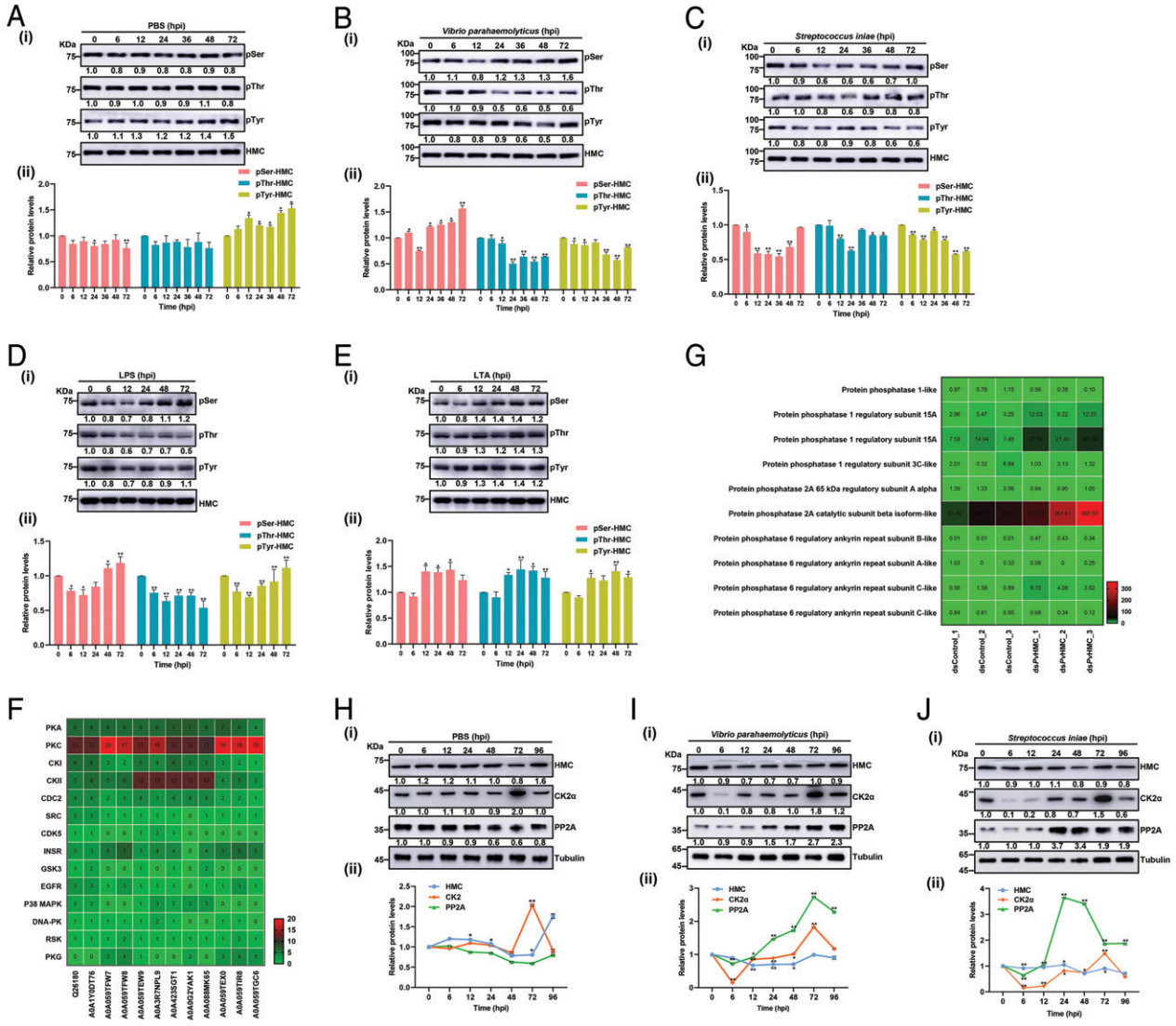

FIGURE 1. Bacterial infection decreases *Pv*HMC phosphorylation. (**A**–**E**) SDS-PAGE and Western blot analysis of serine, threonine, and tyrosine phosphorylation levels of *Pv*HMC at 0, 6, 12, 24, 36, 48, and 72 h postinjection (hpi) with (A) PBS, (B) *Vibrio parahaemolyticus*, (C) *Streptococcus iniae*, (D) LPS, and (E) LTA challenged. (**i**) Western blot analysis and (**ii**) relative gray value analysis. (**F**) Predicted phosphokinases of different variants of *Pv*HMC with their UniProtKB registration numbers. Red to green indicates high to low prediction scores that represent the phosphorylation site of *Pv*HMC corresponding to each kinase. (**G**) Heatmap of differentially expressed protein phosphatases after knockdown *Pv*HMC. (**H**–**J**) SDS-PAGE and Western blot analysis of the expression of *Pv*HMC, *Pv*CK2α, and *Pv*PP2A in shrimp hemocytes at 0, 6, 12, 24, 48, 72, and 96 hpi with (H) PBS, (I) *V. parahaemolyticus*, and (J) *S. iniae* challenge. The data shown are from one of three independent experiments. Statistical significance was analyzed by one-way ANOVA (*$p < 0.05$; **$p < 0.01$). All data are from three independent experiments ($n = 3$) and are shown as mean ± SEM.

p-Ser, p-Thr, and p-Tyr levels of *Pv*HMC in shrimp plasma were observed upon challenge with LPS and LTA. For instance, in response to LPS challenge, the p-Ser and p-Tyr levels of *Pv*HMC in shrimp plasma decreased, followed by an increase. Meanwhile, the p-Thr levels of *Pv*HMC decreased continuously throughout the challenge (Fig. 1D). For LTA treatment, the p-Ser levels of *Pv*HMC in plasma increased from 6 to 12 h, followed by a decrease from 12 to 72 h. The p-Thr levels of *Pv*HMC in shrimp plasma decreased, followed by an increase. However, the p-Tyr increased moderately throughout the challenge period in shrimp plasma (Fig. 1E). Levels of p-Ser and p-Thr of *Pv*HMC in the PBS control group did not change significantly at all time points, whereas p-Tyr levels of *Pv*HMC increased from 12 to 72 h (Fig. 1A). Next, the NetPhos 3.1 server (http://www.cbs.dtu.dk/services/NetPhos/), which is used for predicting Ser, Thr, and Tyr phosphorylation sites on eukaryotic proteins (55), was used to successfully predict 14 kinases (i.e., PKA, PKC, CKI, CKII, CDC2, SRC, CDK5, INSR, GSK3, EFFR, p38 MAPK, DNA-PK, RSK, and PKG) as the putative kinases of *Pv*HMC. Among the predicted kinases, PKC and CKII were among the kinases with the highest scores (Fig. 1F). Additionally, our unpublished MS data of shrimp hepatopancreas immunoprecipitated samples revealed an interaction between the CK2 homolog of *P. vannamei* (*Pv*CK2) and *Pv*HMC (Supplemental Table II). Given that the hepatopancreas in crustaceans integrates immune and metabolic processes (56), we went on to perform in silico screening for the corresponding putative phosphorylases of *Pv*HMC using our in-house unpublished *P. vannamei* hepatopancreas transcriptome data. The screening identified 10 putative protein phosphatases, including protein phosphatase 1 regulatory subunit, protein phosphatase 2A regulatory subunit, PP2AC, and protein phosphatase 6 regulatory subunit among the differentially expressed genes, with PP2AC being the most significantly expressed (Fig. 1G), and it was therefore selected as the potential phosphatase of *Pv*HMC. When shrimp were challenged

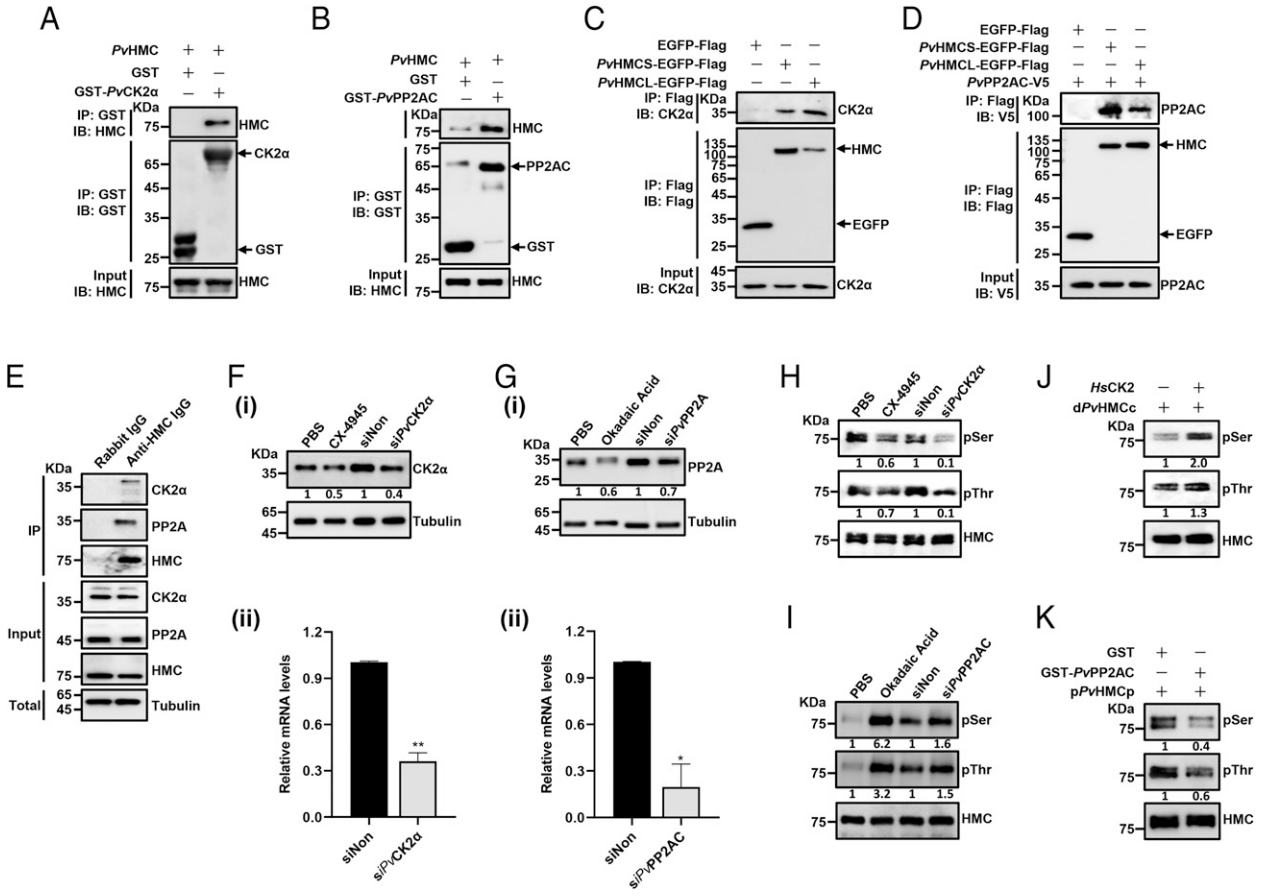

FIGURE 2. *Pv*CK2α and *Pv*PP2AC mediate the phosphorylation and dephosphorylation of *Pv*HMC. (**A** and **B**) In vitro GST pull-down analysis of the interaction of *Pv*HMC with GST-fused tagged (A) *Pv*CK2α and (B) *Pv*PP2AC. (**C**) Immunoprecipitation (IP) and Western blot analysis of Flag-tagged *Pv*HMCS and *Pv*HMCL or endogenous *Drosophila* CK2α overexpressed in *Drosophila* S2 cells. (**D**) Immunoprecipitation and Western blot analysis of Flag-tagged *Pv*HMCS and *Pv*HMCL and V5-tagged *Pv*PP2AC overexpressed in *Drosophila* S2 cells. (**E**) In vivo immunoprecipitation of *Pv*HMC from shrimp hemocyte lysates using anti-*Pv*HMC or IgG (control) Abs followed by immunoblotting using the indicated Abs. (**F**) *Pv*CK2α protein expression (**i**) and transcript levels (**ii**) in shrimp hemocytes after knockdown or inhibitor (CX-4945, 5 μg/shrimp) treatment. (**G**) *Pv*PP2AC protein expression (i) and transcript levels (ii) in shrimp hemocytes after knockdown or inhibitor (OA, 1 μg/shrimp) treatment. (**H**) Phosphorylation level of *Pv*HMC in shrimp plasma after knockdown of *Pv*CK2α or treatment with inhibitor (CX-4945). (**I**) Phosphorylation level of *Pv*HMC in shrimp plasma after knockdown of *Pv*PP2AC or inhibitor (OA) treatment. (**J**) Phosphorylation level of *Pv*HMC in shrimp plasma after treatment of d*Pv*HMCc with human CK2 (*Hs*CK2). (**K**) Phosphorylation level of *Pv*HMC in shrimp plasma after treatment of p-*Pv*HMCp with recombinant GST-*Pv*PP2AC. Data are representative of three independent experiments.

with *V. parahaemolyticus* and *S. iniae*, the protein expression level of *Pv*CK2α in shrimp hemocytes decreased significantly between 6 and 24 h, whereas that of *Pv*PP2AC increased from 24 to 96 h compared with control (Fig. 1H–J, Supplemental Fig. 1B). These results indicate the involvement of *Pv*CK2α and *Pv*PP2A in bacteria-induced phosphorylation and dephosphorylation of *Pv*HMC.

Pv*CK2α and* Pv*PP2AC interact with and modulate*Pv*HMC phosphorylation modification*

The interaction between *Pv*HMC and *Pv*CK2α or *Pv*PP2AC was determined using GST pull-down and Co-IP analyses. *Pv*HMC could interact with *Pv*CK2α (Fig. 2A) and *Pv*PP2AC (Fig. 2B) in vitro. Given that *Pv*CK2α shares high homology with *Drosophila melanogaster*CK2α (84.3%) (47, 57), the interaction between *Pv*HMC and CK2α (*D. melanogaster*CK2α) was performed using *Drosophila* S2 cells overexpressing *Pv*HMC, whereas the interaction between *Pv*HMC and *Pv*PP2AC was carried out using recombinant proteins, due to low homology between *Pv*PP2AC and *D. melanogaster*PP2AC (67.9%) (Supplemental Fig. 1C). The results revealed specific binding of *Pv*HMC with *D. melanogaster* CK2α and *Pv*PP2AC (Fig. 2C, 2D). The interaction between *Pv*HMC and *Pv*CK2α or *Pv*PP2AC was further ascertained using in vivo Co-IP (Fig. 2E). Next, RNAi-mediated knockdown and inhibitor treatment were used to attenuate the expression of *Pv*CK2α and *Pv*PP2AC in shrimp hemocytes followed by determination of plasma *Pv*HMC serine/threonine phosphorylation levels. Knockdown of *Pv*CK2α or inhibitor treatment (Fig. 2F) resulted in decreased serine/threonine phosphorylation levels of *Pv*HMC compared with control (Fig. 2H). In contrast, knockdown of *Pv*PP2AC or inhibitor treatment (Fig. 2G) increased the serine/threonine phosphorylation level of *Pv*HMC compared with control (Fig. 2I). Additionally, in vitro treatment of *Pv*HMC with commercial recombinant human CK2 (*Hs*CK2) increased the phosphorylation level of d*Pv*HMC (Fig. 2J), whereas treatment with recombinant GST-*Pv*PP2AC resulted in the dephosphorylation of phosphorylated *Pv*HMC (p*Pv*HMCp) compared with control (Fig. 2K). These results indicate that *Pv*CK2α and *Pv*PP2AC interact with and modulate the serine/threonine phosphorylation of *Pv*HMC.

Dephosphorylation increases the oxygen-carrying capacity and antibacterial activity of Pv*HMC*

RNAi-mediated knockdown of *Pv*CK2α and *Pv*PP2AC was performed and the effect of *Pv*HMC phosphorylation modification on its oxygen-carrying capacity and antimicrobial activity was determined.

Knockdown of *Pv*CK2α significantly increased the oxygen-carrying capacity of *Pv*HMC compared with control (Supplemental Fig. 2C, 2D). Next, the effect of phosphorylation modification on *Pv*HMC's antibacterial activity (antibacterial assay, bacteria agglutination, and in vitro bacteria binding assay) was explored against Gram-negative (*V. parahaemolyticus*, *V. alginolyticus*, *P. damselae*, and *E. coli*) and Gram-positive (*S. iniae* and *S. aureus*) bacteria using two plasma *Pv*HMC samples with different degrees of phosphorylation (see Fig. 3A). Dephosphorylated *Pv*HMC (i.e., d*Pv*HMCc and d*Pv*HMCp, where "p" represents treated in vitro with recombinant GST-*Pv*PP2AC) had significantly higher bacterial inhibition ratios (Fig. 3B, 3C, Supplemental Fig. 2E, 2F), higher bacteria agglutination activity (Fig. 3D, 3E, Supplemental Fig. 2G, 2H), and stronger bacteria binding affinity (Fig. 3F, 3G) compared with phosphorylated *Pv*HMC (p*Pv*HMCc [where "c" represents treated in vitro with *Hs*CK2] and p*Pv*HMCg [where "g" represents treated in vitro with recombinant GST]). These results indicate that dephosphorylation increased the oxygen-carrying capacity of *Pv*HMC and enhanced its in vitro antibacterial activity.

Several putative phosphorylation sites are found on Pv*HMC*

To identify the phosphorylation sites on *Pv*HMC, three different phosphorylated *Pv*HMC samples (i.e., d*Pv*HMCc, p*Pv*HMCn, and p*Pv*HMCc) prepared (see Fig. 3A) from purified shrimp plasma after knockdown *Pv*CK2α (Fig. 4A) were analyzed by MS (Fig. 4B). Four residues, including Thr^{176}, Ser^{183}, Thr^{507}, and Ser^{548} on the small molecular mass hemocyanin (*Pv*HMCS), and eight residues, that is, Ser^{51}, Ser^{70}, Ser^{191}, Ser^{192}, Ser^{293}, Thr^{517}, Ser^{582}, and Thr^{584} on the large molecular mass hemocyanin (*Pv*HMCL) were identified as specific *Pv*CK2α phosphorylation sites. Among these sites, Thr^{517} on *Pv*HMCL (*Pv*HMCL-T517) had the highest score in p*Pv*HMCn and p*Pv*HMCc, but the lowest score in d*Pv*HMCc (Table I). Thus, *Pv*HMCL-T517 (Fig. 4C) was chosen for further analysis as the potential key site on *Pv*HMC that is phosphorylated by *Pv*CK2α. Next, anti-rabbit polyclonal for *Pv*HMCL with p-Thr^{517} was generated using the peptide c(KLH)NGIKF-pT-FDEGR (Fig. 4D) and used to validate the specificity of this residue. Phosphorylation mimicking mutation (T to E) and dephosphorylation mimicking mutation (T to A) were generated by site-directed mutagenesis at Thr^{517}, and the purified recombinant proteins (*Pv*HMCL-T517A and *Pv*HMCL) expressed in 293T cells were used for the in vitro enzyme assay. As shown in Fig. 4E, *Pv*HMCL was phosphorylated by *Hs*CK2 and dephosphorylated by GST-*Pv*PP2AC, whereas *Pv*HMCL-T517A could not. Similarly, knockdown of *Pv*PP2AC enhanced the phosphorylation of *Pv*HMCL-T517, whereas knockdown of *Pv*CK2α decreased the phosphorylation of *Pv*HMCL-T517 compared with control (Fig. 4F). These results indicate that indeed T517 is the residue on *Pv*HMCL modulated by *Pv*CK2α and *Pv*PP2AC.

Thr^{517} on Pv*HMCL is essential for the antimicrobial activity*

The importance of T517 on the antimicrobial activity of *Pv*HMCL was examined by analyzing the in vitro antibacterial activity of mutant (*Pv*HMCL-T517A and *Pv*HMCL-T517E) and wild-type (*Pv*HMCL) proteins. The mutant protein *Pv*HMCL-T517A had significantly higher bacterial inhibitory activity (Fig. 5A, Supplemental Fig. 2I), agglutination activity (Fig. 5B, Supplemental Fig. 2J), and stronger bacteria binding affinity (Fig. 5C) against *V. parahaemolyticus* and *S. iniae* compared with mutant protein *Pv*HMCL-T517E or wild-type *Pv*HMCL. Similarly, *Pv*HMCL-T517A had significantly strong bacterial (*V. parahaemolyticus* and *S. iniae*) and pathogen-associated molecular patterns (LPS and PGN) binding affinity compared with *Pv*HMCL-T517E or *Pv*HMCL (Fig. 5D, 5E). These results suggest that T517 on *Pv*HMCL is the key phosphorylation residue required for the antibacterial activity of hemocyanin.

To examine whether pathogenic bacteria could also dephosphorylate *Pv*HMCL on T517 in vivo, shrimp were challenged with *V. parahaemolyticus* and *S. iniae* followed by determination of the phosphorylation level of *Pv*HMCL-T517 (Supplemental Fig. 1A) in shrimp plasma. The results revealed a decrease in the phosphorylation level of *Pv*HMCL-T517 over time (Fig. 5F–H) compared with PBS control. Taken together, these results suggest that the dephosphorylation of *Pv*HMCL on residue T517 is crucial for its antibacterial activity.

Discussion

The functional diversity of the arthropodan and molluscan respiratory glycoprotein, hemocyanin, could be attributed to its variant forms (58), transcriptional regulation (59), PTMs (44), and proteolytic degradation to generate different bioactive peptides (38, 46). Glycosylation modification has recently been shown to enhance the antimicrobial activity of hemocyanin in *P. vannamei* (44) and contributes to the structural stability and immunomodulatory properties of molluscan hemocyanin (43). Deacetylation of *P. vannamei* hemocyanin enhances its antibacterial activity by increasing its binding with LPS and destruction of Gram-negative bacteria (27). Among PTMs, protein phosphorylation is the most abundant form (60), which is particularly crucial in cellular signaling (61, 62) and the innate immune response (20). Thus, given that previous studies showed that TSV induces serine phosphorylation of *P. vannamei* hemocyanin (45), we wondered whether phosphorylation modification of *Pv*HMC is essential for its antibacterial activity, as shrimp ponds are inundated with various pathogenic bacteria (63, 64). Accordingly, we found that phosphorylation of hemolymph *Pv*HMC can respond to the stimulation of Gram-negative and Gram-positive bacteria, and upon challenge with LPS and LTA, the overall trend was downregulated, followed by upregulation (Fig. 1B–E), suggesting that protein phosphorylation could be vital in modulating the antimicrobial activity of *Pv*HMC, which is consistent with previous studies in mammals where different pathogen stimulations led to different responses and changes in different phosphorylation types of the same protein, such as TANK binding kinase 1 (TBK1) (65), STAT (66), and NF-κB (67). However, the main reason for this phosphorylation of these factors is that their upstream kinases or phosphatases change under pathogen stimulation (20). Therefore, it is necessary to explore which kinases or phosphatases that lead to *Pv*HMC produce different phosphorylation modifications under different pathogen stimulation.

In this study, we showed that serine and threonine phosphorylation of *Pv*HMC, which is modulated by the shrimp homologs of CK2α and PP2AC (i.e., *Pv*CK2α and *Pv*PP2AC), is a key feature in the antibacterial activity of *Pv*HMC. In silico analysis revealed *Pv*CK2α and *Pv*PP2AC as the potential kinase and phosphatase, respectively, that modify *Pv*HMC, whereas protein levels of *Pv*CK2α and *Pv*PP2AC responded to bacterial challenge in a similar pattern as the corresponding phosphorylation modification of *Pv*HMC (Fig. 1G, 1H). These findings indicate that *Pv*HMC undergoes serine and threonine phosphorylation modulated by *Pv*CK2α and *Pv*PP2AC during the antibacterial response in penaeid shrimp, which is consistent with previous studies in mammals where CK2 mediates the phosphorylation of human RIG-I to enhance the antiviral (Sendai virus) immune response (68) or RIG-I–mediated antiviral (human herpesvirus and Sendai virus) immunity in humans, mediated by protein phosphatase 6 catalytic subunit (PPP6C) (69). Similarly, *Streptococcus pneumoniae* can activate protein phosphatase 1 (PP1) to induce the dephosphorylation of histone H3 in A549 lung epithelial cells as an intracellular

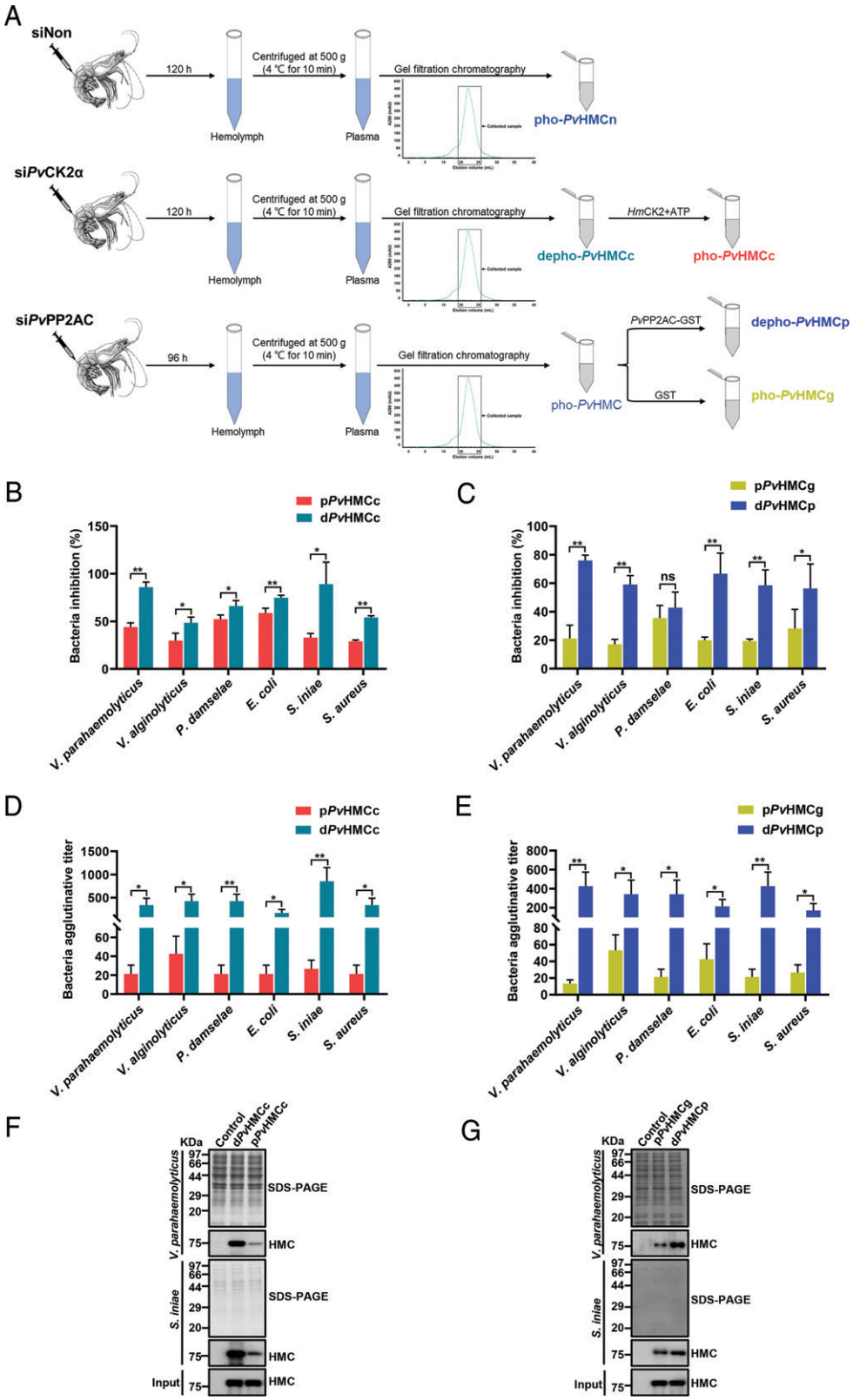

FIGURE 3. Phosphorylation of *Pv*HMC attenuates its antimicrobial activity. (**A**) Steps used in the preparation of different phosphorylated samples of *Pv*HMC. Sample designations are as follows: d*Pv*HMCc, *Pv*HMC samples dephosphorylated by *Pv*CK2α knockdown; d*Pv*HMCp, dephosphorylated purified plasma *Pv*HMC treated in vitro with recombinant GST-*Pv*PP2AC; p*Pv*HMCc, phosphorylated samples of d*Pv*HMCc treated in vitro with *Hs*CK2; p*Pv*HMCg, phosphorylated purified plasma *Pv*HMC treated in vitro with recombinant GST; p*Pv*HMCp, phosphorylated samples of *Pv*HMC after *Pv*PP2AC knockdown; p*Pv*HMCn, *Pv*HMC samples from control siNon-injected shrimp. (**B** and **C**) Bacterial inhibition of different phosphorylated *Pv*HMC samples (B) p*Pv*HMCc and d*Pv*HMCc and (C) p*Pv*HMCg and d*Pv*HMCp against *V. parahaemolyticus*, *V. alginolyticus*, *P. damselae*, *E. coli*, *S. iniae*, and *S. aureus*. (**D** and **E**) Bacterial agglutinative activity of different phosphorylated *Pv*HMC samples (D) p*Pv*HMCc and d*Pv*HMCc and (E) p*Pv*HMCg and d*Pv*HMCp against *V. parahaemolyticus*, *V. alginolyticus*, *P. damselae*, *E. coli*, *S. iniae*, and *S. aureus*. (**F** and **G**) Bacterial binding affinity of different phosphorylated *Pv*HMC samples (F) p*Pv*HMCc and d*Pv*HMCc and (G) p*Pv*HMCg and d*Pv*HMCp with *V. parahaemolyticus* and *S. iniae* determined by Western blot. Proteins were used at a concentration of 200 μg/ml. Statistical significance was analyzed by one-way ANOVA (*$p < 0.05$; **$p < 0.01$; ns, not significant). All data are from three independent experiments with biological duplicates in each ($n = 3$) and shown as mean ± SEM.

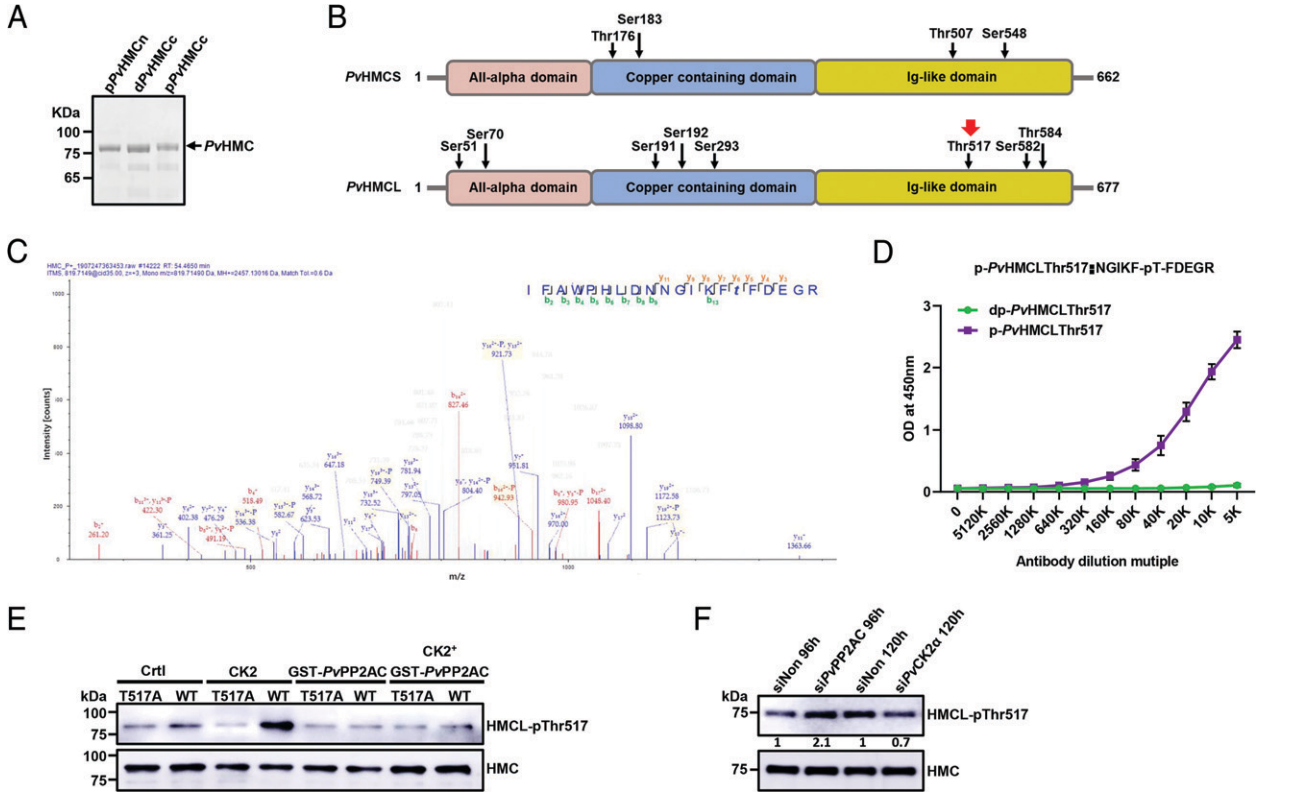

FIGURE 4. *Pv*CK2α and *Pv*PP2AC modulate the phosphorylation of *Pv*HMC on Thr^{517}. (**A**) Gel filtration chromatography purified hemocyanin (d*Pv*HMCc) from hemolymph of *Pv*CK2α knockdown shrimp followed by in vitro kinase assay with or without *Hs*CK2. (**B**) Mapping of phosphorylation sites on *Pv*HMC associated with CK2 based on LTQ-Orbitrap XL mass spectrometry. (**C**) Mass spectrum of CK2-phosphorylated *Pv*HMCL Thr^{517} peptide sequence. The position of phosphorylated Thr^{517} (pT) and the "b" and "y" ions are shown. (**D**) ELISA analysis of anti–p-*Pv*HMC-T517, p-*Pv*HMC-T517: Thr^{517} phosphorylated peptide, and dp-*Pv*HMC-T517 nonphosphorylated peptide. Data shown are representative of three independent experiments. (**E**) Validation of p-T517-*Pv*HMCL Ab using recombinant *Pv*HMCL-Flag (wild-type) and mutant proteins treated in vitro with recombinant *Hs*CK2α or recombinant *Pv*PP2AC-GST. Data are representative of three independent experiments. (**F**) Phosphorylation level of plasma *Pv*HMCL-T517 after *Pv*PP2AC or *Pv*CK2α knockdown and determined by Western blot.

strategy to escape the host immune response (70). Thus, *Pv*CK2α and *Pv*PP2AC regulate the phosphorylation of *Pv*HMC to modulate its antibacterial activity.

With >500 substrates, CK2, a highly conserved serine/threonine kinase (71, 72), phosphorylates key proteins to regulate numerous cellular processes, including inflammation (73) and immunity (72). Similarly, PP2ACα, a highly complex heterotrimeric enzyme that catalyzes the selective removal of phosphate groups from serine and threonine residues, has been implicated in inflammatory or immune responses through phosphorylation modifications of its substrates (74). We found that *Pv*CK2α interacted with and phosphorylated *Pv*HMC (Fig. 2) thereby attenuating the oxygen-binding capacity and antibacterial activity of *Pv*HMC (Fig. 3). Conversely, interaction of *Pv*PP2AC with *Pv*HMC resulted in dephosphorylation (Fig. 2) but enhancement of antibacterial activity of *Pv*HMC (Fig. 3). These results, although not previously observed in crustaceans, are consistent with mammalian studies, where the function of some key proteins was regulated by phosphorylation modification by kinase/phosphatase pairs. For instance, human CK2 mediates the phosphorylation of the co-chaperone FNIP1 to increase the inhibition of Hsp90 ATPase activity, which gradually activates both the kinase and nonkinase components of

Table I. Summary of mass spectrometry data of the phosphorylation sites on *Pv*HMC modulated by CK2

Hemocyanin	Sequence Motif	Phosphorylation Sites	Highest PTM Score		
			d*Pv*HMCc	p*Pv*HMCn	p*Pv*HMCc
HMCS	RAKQKQ**T**PGKFKS	Thr^{176}	—	—	100
A0A1Y0DT76	PGKFKS**S**FTGTKK	Ser^{183}	49.5	—	99.2
	NNGIEY**T**FDEGRW	Thr^{507}	74	—	99.3
	TVPDVP**S**IHDLFA	Ser^{548}	—	—	100
HMCL	YGNIRD**S**DLKAKA	Ser^{51}	—	—	99.5
A0A059TEW9	ADLSHY**S**DGGEAV	Ser^{70}	44.2	1.9	100
	KPGKFK**S**SFTGTK	Ser^{191}	—	—	76.9
	PGKFKS**S**FTGTKK	Ser^{192}	—	—	76.9
	YGGQFP**S**RPDNVD	Ser^{293}	—	—	100
	NNGIKF**T**FDEGRW	Thr^{517}	—	100	100
	GLKDFE**S**ATGIPN	Ser^{582}	—	—	100
	KDFESA**T**GIPNRF	Thr^{584}	—	—	50

S/T denote phosphorylated Ser/Thr residues present within the consensus motifs of hemocyanin; "—" indicates no PTM score.

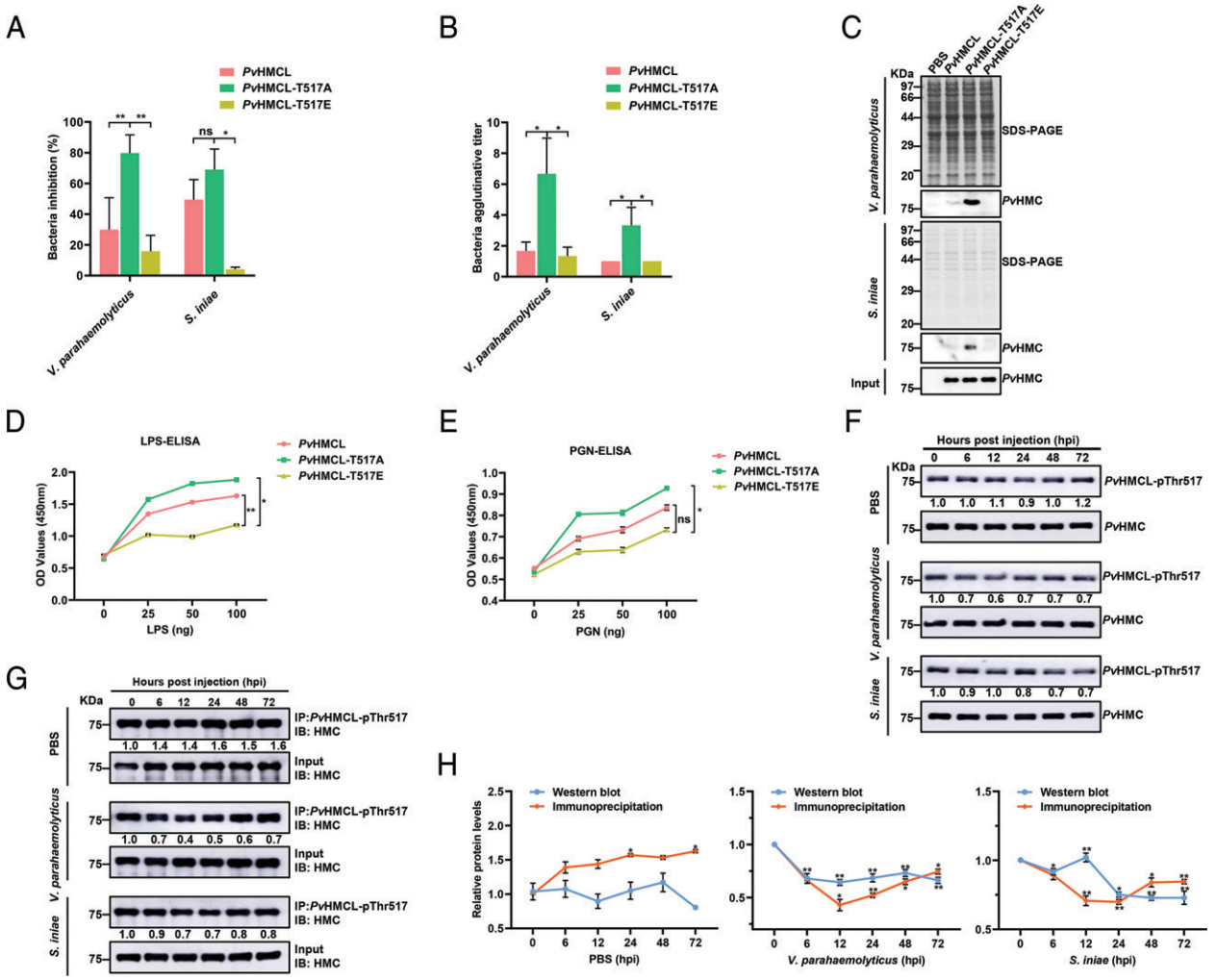

FIGURE 5. Phosphorylation modification of *Pv*HMCL-T517 is important for antibacterial response. (**A**) Bacterial inhibition of *Pv*HMCL, *Pv*HMCL-T517A, and *Pv*HMCL-T517E against *V. parahaemolyticus* and *S. iniae*. Proteins were used at a concentration of 50 μg/ml. (**B**) Bacterial agglutination activity of *Pv*HMCL, *Pv*HMCL-T517A, and *Pv*HMCL-T517E with *V. parahaemolyticus* and *S. iniae* with or without calcium. (**C**) Bacterial binding activity of *Pv*HMCL, *Pv*HMCL-T517A, and *Pv*HMCL-T517E with *V. parahaemolyticus* and *S. iniae* determined by Western blot. (**D** and **E**) Interaction of recombinant *Pv*HMCL protein with LPS and PGN analyzed by ELISA. Plates were coated with pathogen-associated molecular patterns (LPS and PGN) and incubated with *Pv*HMCL, *Pv*HMCL-T517A, or *Pv*HMCL-T517E followed by anti-*Pv*HMC antiserum, and signals were detected with anti-rabbit IgG secondary Ab at 450 nm. (**F**) SDS-PAGE and Western blot analysis of *Pv*HMCL-T517 phosphorylation at 0, 12, 24, 48, and 72 h postinjection (hpi) with PBS, *V. parahaemolyticus*, or *S. iniae*. (**G**) Immunoprecipitation and immunoblot analysis of plasma from shrimp infected with *V. parahaemolyticus* or *S. iniae* at the indicated time points and probed with *Pv*HMCL-p-Thr^{517} Ab. (**H**) Relative gray value analysis of (F) and (G). Statistical significance was analyzed by one-way ANOVA (*p <0.05; **p <0.01; ns, not significant). All data are from three independent experiments with biological duplicates in each (n = 3) and shown as mean ± SEM.

the enzyme and the activity of protein phosphatase 5 (PP5) to dephosphorylate FNIP1, resulting in its degradation (75). Similarly, the phosphorylation of somatic nuclear autoantigenic sperm protein (sNASP) by CK2 is essential for proinflammatory cytokine production, especially in bacterial infection, whereas directly recruited PP4 dephosphorylates p-sNASP to inhibit sNASP-dependent proinflammatory cytokine production and downstream signaling following bacterial LPS treatment (76). These results indicate that the antibacterial activity and oxygen-binding capacity of *Pv*HMC is enhanced when dephosphorylated. Although the C-terminal of *Pv*HMC was previously reported to be phosphorylated by the ERK1/2 kinase as part of the shrimp antiviral (TSV) response (45), the consequence of this phosphorylation modification on the primordial function of hemocyanin, that is, oxygen carriage, and the corresponding phosphatase or effect on bacterial pathogens were not explored. Indeed, *Pv*CK2α and *Pv*PP2AC modulate the phosphorylation of hemocyanin to affect its functions (oxygen carriage and antimicrobial activity), given that PTMs can change the net protein charge to affect antimicrobial activity (27, 77), modify protein solubility (78), or change protein structure to alter its functions (79). Indeed, the details of this relationship and the molecular mechanisms involved require further studies, especially when crystallographic structures of *Pv*HMC are available.

In both vertebrates and invertebrates, protein phosphorylation modification mediated by kinases and phosphatases on specific residues of host proteins, such as FOXO3 on Ser^{574} in human monocytic cells in response to LPS stimulation (80), TRAF3 on Ser^{438} in HEK293T cells upon vesicular stomatitis virus infection (50), and IRF3 on Ser^{396} in 293T cells after LPS, polyinosinic-polycytidylic acid, and Sendai virus challenge (81), plays a pivotal role in immune responses. During HIV-1 infection, cyclin-dependent kinase 1 (CDK1)–mediated phosphorylation of SAMHD1 (sterile α motif domain and HD domain–containing protein 1) on Thr^{592} attenuate its ability to inhibit HIV-1 replication in 293T or HeLa cells (82).

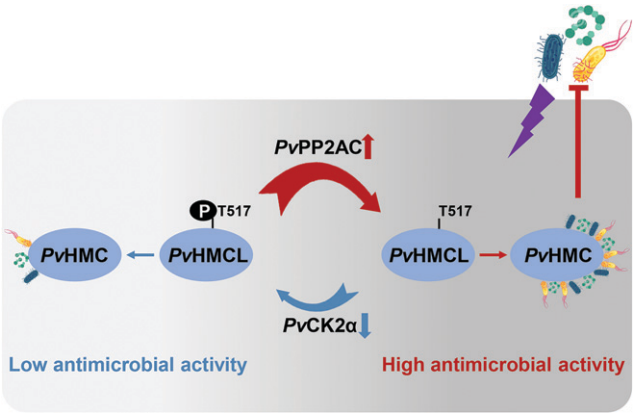

FIGURE 6. Phosphorylation modification of hemocyanin on Thr^{517} mediated by CK2α and PP2AC is critical for antibacterial activity in *Penaeus vannamei.*

However, PP2A-B55α dephosphorylates SAMHD1 on Thr^{592} to activate SAMHD1, thereby restricting HIV-1 replication (83). Accordingly, Thr^{517} on *Pv*HMCL was identified in the current study as the key residue that upon phosphorylation modification by *Pv*CK2α and *Pv*PP2AC (Fig. 4) alters the functions of hemocyanin. For instance, whereas wild-type *Pv*HMC and the phosphorylation mimic *Pv*HMCL-T517E both exhibited weak antimicrobial activities (i.e., agglutinative and bacterial binding) against *V. parahaemolyticus* and *S. iniae*, the dephosphorylation mimic *Pv*HMCL-T517A had significantly enhanced antibacterial activity (Fig. 5A, 5B) and higher bacterial binding capacity compared with *Pv*HMCL-T517E or *Pv*HMCL (Fig. 5C–E). Furthermore, the phosphorylation level of *Pv*HMCL-T517 was decreased over time after challenge with *V. parahaemolyticus* or *S. iniae* compared with PBS control (Fig. 5F–H). The modulation of hemocyanin's function is surely not limited to this single residue (Thr^{517}), given that glycosylation of Thr^{537}, Ser^{539}, and Thr^{542} on the C terminus of hemocyanin is associated with the antimicrobial immune activity in *P. vannamei* (44). The acetylation of K481 and K484 attenuates *P. vannamei* hemocyanin binding with LPS and its antibacterial activity (27). These results are synonymous with previous studies where the white spot syndrome virus protein kinase WSV083 was reported to phosphorylate nuclear DNA-binding TCF protein on Thr^{39} and Thr^{104} in *P. vannamei* to suppress antiviral activity (84), whereas the glycosylation of *Helix pomatia* hemocyanin on Asn^{387} affected its immunological cross-reactivity with α-macroglobulin (85), and glycosylation of *R. venosa* hemocyanin on 331–333 (Asn-Asp-Thr) enhanced its antiviral activity against respiratory syncytial virus (32). Taken together, these results provide strong evidence that phosphorylation of *Pv*HMC on T517 is crucial for modulating its functions, especially its antibacterial activity (Fig. 6). Nonetheless, given that *Pv*HMCL-T517E still has antibacterial activity, it cannot be ruled out that the phosphorylation of other sites contributes to the overall antimicrobial activity of hemocyanin (*Pv*HMC), and hence future studies should attempt to delineate the contributions of these other phosphorylation sites.

In conclusion, this study reveals that the phosphorylation modification of *Pv*HMC by *Pv*CK2α and *Pv*PP2AC modulates its oxygen-carrying capacity and antibacterial activity. Most importantly, the T517 residue on *Pv*HMCL is a critical site, and hence its phosphorylation modification alters the key functions of hemocyanin in *P. vannamei* and possibly in other crustaceans. Despite the novelty of these findings, whether the phosphorylation of T517 synergistically enhances the functions of hemocyanin remains to be clarified, given that other serine/threonine residues are located in the vicinity of T517.

Disclosures

The authors have no financial conflicts of interest.

References

1. Milutinović, B., and J. Kurtz. 2016. Immune memory in invertebrates. *Semin. Immunol.* 28: 328–342.
2. Cherry, S., and N. Silverman. 2006. Host-pathogen interactions in *Drosophila*: new tricks from an old friend. *Nat. Immunol.* 7: 911–917.
3. Stuart, L. M., and R. A. Ezekowitz. 2008. Phagocytosis and comparative innate immunity: learning on the fly. *Nat. Rev. Immunol.* 8: 131–141.
4. Zhang, Z., J. J. Aweya, D. Yao, Z. Zheng, N. T. Tran, S. Li, and Y. Zhang. 2021. Ubiquitination as an important host-immune response strategy in penaeid shrimp: inferences from other species. *Front. Immunol.* 12: 697397.
5. Aweya, J. J., Z. H. Zheng, X. Y. Zheng, D. F. Yao, and Y. L. Zhang. 2021. The expanding repertoire of immune-related molecules with antimicrobial activity in penaeid shrimps: a review. *Rev. Aquacult.* 13: 1907–1937.
6. Becker, T., G. Loch, M. Beyer, I. Zinke, A. C. Aschenbrenner, P. Carrera, T. Inhester, J. L. Schultze, and M. Hoch. 2010. FOXO-dependent regulation of innate immune homeostasis. *Nature* 463: 369–373.
7. Watson, F. L., R. Püttmann-Holgado, F. Thomas, D. L. Lamar, M. Hughes, M. Kondo, V. I. Rebel, and D. Schmucker. 2005. Extensive diversity of Ig-superfamily proteins in the immune system of insects. *Science* 309: 1874–1878.
8. Li, X. J., L. Yang, D. Li, Y. T. Zhu, Q. Wang, and W. W. Li. 2018. Pathogen-specific binding soluble down syndrome cell adhesion molecule (Dscam) regulates phagocytosis via membrane-bound Dscam in crab. *Front. Immunol.* 9: 801.
9. Pinaud, S., J. Portela, D. Duval, F. C. Nowacki, M. A. Olive, J. F. Allienne, R. Galinier, N. M. Dheilly, S. Kieffer-Jaquinod, G. Mitta, et al. 2016. A shift from cellular to humoral responses contributes to innate immune memory in the vector snail *Biomphalaria glabrata*. *PLoS Pathog.* 12: e1005361.
10. Hanington, P. C., and S. M. Zhang. 2011. The primary role of fibrinogen-related proteins in invertebrates is defense, not coagulation. *J. Innate Immun.* 3: 17–27.
11. Zhang, S. M., C. M. Adema, T. B. Kepler, and E. S. Loker. 2004. Diversification of Ig superfamily genes in an invertebrate. *Science* 305: 251–254.
12. Wang, X. W., and J. X. Wang. 2013. Diversity and multiple functions of lectins in shrimp immunity. *Dev. Comp. Immunol.* 39: 27–38.
13. Donpudsa, S., S. Visetnan, P. Supungul, S. Tang, A. Tassanakajon, and V. Rimphanitchayakit. 2014. Type I and type II crustins from *Penaeus monodon*, genetic variation and antimicrobial activity of the most abundant crustinPm4. *Dev. Comp. Immunol.* 47: 95–103.
14. Arayamethakorn, S., P. Supungul, A. Tassanakajon, and K. Krusong. 2017. Characterization of molecular properties and regulatory pathways of Crustin*Pm*1 and Crustin*Pm*7 from the black tiger shrimp *Penaeus monodon*. *Dev. Comp. Immunol.* 67: 18–29.
15. Xiao, B., Q. Fu, S. Niu, P. Zhu, J. He, and C. Li. 2020. Penaeidins restrict white spot syndrome virus infection by antagonizing the envelope proteins to block viral entry. *Emerg. Microbes Infect.* 9: 390–412.
16. Destoumieux-Garzón, D., R. D. Rosa, P. Schmitt, C. Barreto, J. Vidal-Dupiol, G. Mitta, Y. Gueguen, and E. Bachère. 2016. Antimicrobial peptides in marine invertebrate health and disease. *Philos. Trans. R. Soc. Lond. B Biol. Sci.* 371: 205–211.
17. de Jongh, R. P. H., A. D. J. van Dijk, M. K. Julsing, P. J. Schaap, and D. de Ridder. 2020. Designing eukaryotic gene expression regulation using machine learning. *Trends Biotechnol.* 38: 191–201.
18. Wang, W., A. Li, Z. Zhang, and C. Chu. 2021. Posttranslational modifications: regulation of nitrogen utilization and signaling. *Plant Cell Physiol.* 62: 543–552.
19. Deribe, Y. L., T. Pawson, and I. Dikic. 2010. Post-translational modifications in signal integration. *Nat. Struct. Mol. Biol.* 17: 666–672.
20. Liu, J., C. Qian, and X. Cao. 2016. Post-translational modification control of innate immunity. *Immunity* 45: 15–30.
21. Meinander, A., C. Runchel, T. Tenev, L. Chen, C. H. Kim, P. S. Ribeiro, M. Broemer, F. Leulier, M. Zvelebil, N. Silverman, and P. Meier. 2012. Ubiquitylation of the initiator caspase DREDD is required for innate immune signalling. *EMBO J.* 31: 2770–2783.
22. Jugder, B. E., L. Kamareddine, and P. I. Watnick. 2021. Microbiota-derived acetate activates intestinal innate immunity via the Tip60 histone acetyltransferase complex. *Immunity* 54: 1683–1697.e3.
23. Chen, K., X. Luan, Q. Liu, J. Wang, X. Chang, A. M. Snijders, J. H. Mao, J. Secombe, Z. Dan, J. H. Chen, et al. 2019. *Drosophila* histone demethylase KDM5 regulates social behavior through immune control and gut microbiota maintenance. *Cell Host Microbe* 25: 537–552.e8.
24. Ouvry-Patat, S. A., and K. L. Schey. 2007. Characterization of antimicrobial histone sequences and posttranslational modifications by mass spectrometry. *J. Mass Spectrom.* 42: 664–674.
25. Lu, H., L. Ruan, and X. Xu. 2011. An immediate-early protein of white spot syndrome virus modulates the phosphorylation of focal adhesion kinase of shrimp. *Virology* 419: 84–89.
26. Li, D., Z. Wan, X. Li, M. Duan, L. Yang, Z. Ruan, Q. Wang, and W. Li. 2019. Alternatively spliced down syndrome cell adhesion molecule (Dscam) controls innate immunity in crab. *J. Biol. Chem.* 294: 16440–16450.
27. Nie, J., J. J. Aweya, Z. Yu, H. Zhou, F. Wang, D. Yao, Z. Zheng, S. Li, H. Ma, and Y. Zhang. 2022. Deacetylation of K481 and K484 on penaeid shrimp hemocyanin is critical for antibacterial activity. *J. Immunol.* 209: 476–487.
28. Coates, C. J., E. L. Bradford, C. A. Krome, and J. Nairn. 2012. Effect of temperature on biochemical and cellular properties of captive *Limulus polyphemus*. *Aquaculture* 334–337: 30–38.

29. Decker, H., N. Hellmann, E. Jaenicke, B. Lieb, U. Meissner, and J. Markl. 2007. Minireview: recent progress in hemocyanin research. *Integr. Comp. Biol.* 47: 631–644.
30. Coates, C. J., and J. Nairn. 2014. Diverse immune functions of hemocyanins. *Dev. Comp. Immunol.* 45: 43–55.
31. Yao, T., M. M. Zhao, J. He, T. Han, W. Peng, H. Zhang, J. Y. Wang, and J. Z. Jiang. 2019. Gene expression and phenoloxidase activities of hemocyanin isoforms in response to pathogen infections in abalone *Haliotis diversicolor*. *Int. J. Biol. Macromol.* 129: 538–551.
32. Dolashka-Angelova, P., B. Lieb, L. Velkova, N. Heilen, K. Sandra, L. Nikolaeva-Glomb, A. Dolashki, A. S. Galabov, J. Van Beeumen, S. Stevanovic, et al. 2009. Identification of glycosylated sites in *Rapana* hemocyanin by mass spectrometry and gene sequence, and their antiviral effect. *Bioconjug. Chem.* 20: 1315–1322.
33. Jiang, N., N. S. Tan, B. Ho, and J. L. Ding. 2007. Respiratory protein-generated reactive oxygen species as an antimicrobial strategy. *Nat. Immunol.* 8: 1114–1122.
34. Zhang, Y., S. Wang, A. Xu, J. Chen, B. Lin, and X. Peng. 2006. Affinity proteomic approach for identification of an IgA-like protein in *Litopenaeus vannamei* and study on its agglutination characterization. *J. Proteome Res.* 5: 815–821.
35. Zhang, Y., F. Yan, Z. Hu, X. Zhao, S. Min, Z. Du, S. Zhao, X. Ye, and Y. Li. 2009. Hemocyanin from shrimp *Litopenaeus vannamei* shows hemolytic activity. *Fish Shellfish Immunol.* 27: 330–335.
36. Liu, S., J. J. Aweya, L. Zheng, Z. Zheng, H. Huang, F. Wang, D. Yao, T. Ou, and Y. Zhang. 2022. LvHemB1, a novel cationic antimicrobial peptide derived from the hemocyanin of *Litopenaeus vannamei*, induces cancer cell death by targeting mitochondrial voltage-dependent anion channel 1. *Cell Biol. Toxicol.* 38: 87–110.
37. Wen, Y., S. Zhan, H. Huang, M. Zhong, J. Chen, C. You, F. Wang, and Y. Zhang. 2016. Identification and characterization of an 18.4kDa antimicrobial truncation from shrimp *Litopenaeus vannamei* hemocyanin upon *Vibrio parahaemolyticus* infection. *Fish Shellfish Immunol.* 56: 450–458.
38. Zhan, S., J. J. Aweya, F. Wang, D. Yao, M. Zhong, J. Chen, S. Li, and Y. Zhang. 2019. *Litopenaeus vannamei* attenuates white spot syndrome virus replication by specific antiviral peptides generated from hemocyanin. *Dev. Comp. Immunol.* 91: 50–61.
39. Aweya, J. J., K. Zhuang, Y. Liu, J. Fan, D. Yao, F. Wang, X. Chen, S. Li, H. Ma, and Y. Zhang. 2022. The ARM repeat domain of hemocyanin interacts with MKK4 to modulate antimicrobial peptides expression. *iScience* 25: 103958.
40. Zhao, X., L. Guo, Y. Zhang, Y. Liu, X. Zhang, J. Lun, J. Chen, and Y. Li. 2012. SNPs of hemocyanin C-terminal fragment in shrimp *Litopenaeus vannamei*. *FEBS Lett.* 586: 403–410.
41. Fan, J., X. Li, H. Lu, R. Lin, J. J. Aweya, and Y. Zhang. 2019. N-terminal diversity of *Litopenaeus vannamei* hemocyanin and immunity. *Mol. Immunol.* 112: 360–368.
42. Zhao, S., X. Lu, Y. Zhang, X. Zhao, M. Zhong, S. Li, and J. Lun. 2013. Identification of a novel alternative splicing variant of hemocyanin from shrimp *Litopenaeus vannamei*. *Immunol. Lett.* 154: 1–6.
43. Salazar, M. L., J. M. Jiménez, J. Villar, M. Rivera, M. Báez, A. Manubens, and M. I. Becker. 2019. *N*-Glycosylation of mollusk hemocyanins contributes to their structural stability and immunomodulatory properties in mammals. *J. Biol. Chem.* 294: 19546–19564.
44. Zhang, Z., R. Li, J. J. Aweya, F. Wang, M. Zhong, and Y. Zhang. 2019. Identification and characterization of glycosylation sites on *Litopenaeus vannamei* hemocyanin. *FEBS Lett.* 593: 820–830.
45. Havanapan, P. O., R. Kanlaya, A. Bourchookarn, C. Krittanai, and V. Thongboonkerd. 2009. C-terminal hemocyanin from hemocytes of *Penaeus vannamei* interacts with ERK1/2 and undergoes serine phosphorylation. *J. Proteome Res.* 8: 2476–2483.
46. Li, C., F. Wang, J. J. Aweya, D. Yao, Z. Zheng, H. Huang, S. Li, and Y. Zhang. 2018. Trypsin of *Litopenaeus vannamei* is required for the generation of hemocyanin-derived peptides. *Dev. Comp. Immunol.* 79: 95–104.
47. Feng, Q., Y. Huang, D. Yao, C. Zhu, S. Li, H. Ma, J. J. Aweya, and Y. Zhang. 2019. *Litopenaeus vannamei* CK2 is involved in shrimp innate immunity by modulating hemocytes apoptosis. *Fish Shellfish Immunol.* 94: 643–653.
48. Livak, K. J., and T. D. Schmittgen. 2001. Analysis of relative gene expression data using real-time quantitative PCR and the $2^{-\Delta\Delta C(T)}$ method. *Methods* 25: 402–408.
49. Tao, M., H. Zhou, K. Luo, J. Lu, Y. Zhang, and F. Wang. 2019. Quantitative serum proteomics analyses reveal shrimp responses against WSSV infection. *Dev. Comp. Immunol.* 93: 89–92.
50. Zhou, Y., C. He, D. Yan, F. Liu, H. Liu, J. Chen, T. Cao, M. Zuo, P. Wang, Y. Ge, et al. 2016. The kinase CK1ε controls the antiviral immune response by phosphorylating the signaling adaptor TRAF3. *Nat. Immunol.* 17: 397–405.
51. Wu, J. L., H. Y. Wu, D. Y. Tsai, M. F. Chiang, Y. J. Chen, S. Gao, C. C. Lin, C. H. Lin, K. H. Khoo, Y. J. Chen, and K. I. Lin. 2016. Temporal regulation of Lsp1 *O*-GlcNAcylation and phosphorylation during apoptosis of activated B cells. *Nat. Commun.* 7: 12526.
52. Hagner-Holler, S., A. Schoen, W. Erker, J. H. Marden, R. Rupprecht, H. Decker, and T. Burmester. 2004. A respiratory hemocyanin from an insect. *Proc. Natl. Acad. Sci. USA* 101: 871–874.
53. Zhang, Y. L., B. Peng, H. Li, F. Yan, H. K. Wu, X. L. Zhao, X. M. Lin, S. Y. Min, Y. Y. Gao, S. Y. Wang, et al. 2017. C-terminal domain of hemocyanin, a major antimicrobial protein from *Litopenaeus vannamei*: structural homology with immunoglobulins and molecular diversity. *Front. Immunol.* 8: 611.
54. Wang, X. W., X. F. Zhao, and J. X. Wang. 2014. C-type lectin binds to β-integrin to promote hemocytic phagocytosis in an invertebrate. *J. Biol. Chem.* 289: 2405–2414.
55. Blom, N., T. Sicheritz-Pontén, R. Gupta, S. Gammeltoft, and S. Brunak. 2004. Prediction of post-translational glycosylation and phosphorylation of proteins from the amino acid sequence. *Proteomics* 4: 1633–1649.
56. Rőszer, T. 2014. The invertebrate midintestinal gland ("hepatopancreas") is an evolutionary forerunner in the integration of immunity and metabolism. *Cell Tissue Res.* 358: 685–695.
57. Lassmann, T., and E. L. Sonnhammer. 2005. Automatic assessment of alignment quality. *Nucleic Acids Res.* 33: 7120–7128.
58. Zhao, X., L. Guo, X. Lu, H. Lu, F. Wang, M. Zhong, J. Chen, and Y. Zhang. 2016. Evidences of abundant hemocyanin variants in shrimp *Litopenaeus vannamei*. *Mol. Immunol.* 77: 103–112.
59. Yang, P., D. Yao, J. J. Aweya, F. Wang, P. Ning, S. Li, H. Ma, and Y. Zhang. 2019. c-Jun regulates the promoter of small subunit hemocyanin gene of *Litopenaeus vannamei*. *Fish Shellfish Immunol.* 84: 639–647.
60. Silva-Sanchez, C., H. Li, and S. Chen. 2015. Recent advances and challenges in plant phosphoproteomics. *Proteomics* 15: 1127–1141.
61. Niehrs, C. 2012. The complex world of WNT receptor signalling. *Nat. Rev. Mol. Cell Biol.* 13: 767–779.
62. Ardito, F., M. Giuliani, D. Perrone, G. Troiano, and L. Lo Muzio. 2017. The crucial role of protein phosphorylation in cell signaling and its use as targeted therapy (Review). *Int. J. Mol. Med.* 40: 271–280.
63. Flegel, T. W. 2012. Historic emergence, impact and current status of shrimp pathogens in Asia. *J. Invertebr. Pathol.* 110: 166–173.
64. Tran, L., L. Nunan, R. M. Redman, L. L. Mohney, C. R. Pantoja, K. Fitzsimmons, and D. V. Lightner. 2013. Determination of the infectious nature of the agent of acute hepatopancreatic necrosis syndrome affecting penaeid shrimp. *Dis. Aquat. Organ.* 105: 45–55.
65. Liu, S., X. Cai, J. Wu, Q. Cong, X. Chen, T. Li, F. Du, J. Ren, Y.-T. Wu, N. V. Grishin, and Z. J. Chen. 2015. Phosphorylation of innate immune adaptor proteins MAVS, STING, and TRIF induces IRF3 activation. *Science* 347: aaa2630.
66. Stark, G. R., and J. E. Darnell, Jr. 2012. The JAK-STAT pathway at twenty. *Immunity* 36: 503–514.
67. Wang, N., R. Wu, D. Tang, and R. Kang. 2021. The BET family in immunity and disease. *Signal Transduct. Target. Ther.* 6: 23.
68. Sun, Z., H. Ren, Y. Liu, J. L. Teeling, and J. Gu. 2011. Phosphorylation of RIG-I by casein kinase II inhibits its antiviral response. *J. Virol.* 85: 1036–1047.
69. Tan, P., L. He, J. Cui, C. Qian, X. Cao, M. Lin, Q. Zhu, Y. Li, C. Xing, X. Yu, et al. 2017. Assembly of the WHIP-TRIM14-PPP6C mitochondrial complex promotes RIG-I-mediated antiviral signaling. *Mol. Cell* 68: 293–307.e5.
70. Dong, W., O. Rasid, C. Chevalier, M. Connor, M. J. G. Eldridge, and M. A. Hamon. 2020. *Streptococcus pneumoniae* infection promotes histone H3 dephosphorylation by modulating host PP1 phosphatase. *Cell Rep.* 30: 4016–4026.e4.
71. Borgo, C., and M. Ruzzene. 2019. Role of protein kinase CK2 in antitumor drug resistance. *J. Exp. Clin. Cancer Res.* 38: 287.
72. Gibson, S. A., and E. N. Benveniste. 2018. Protein kinase CK2: an emerging regulator of immunity. *Trends Immunol.* 39: 82–85.
73. Yang, F. M., Y. Zuo, W. Zhou, C. Xia, B. Hahm, M. Sullivan, J. Cheng, H. M. Chang, and E. T. Yeh. 2018. sNASP inhibits TLR signaling to regulate immune response in sepsis. *J. Clin. Invest.* 128: 2459–2472.
74. Clark, A. R., and M. Ohlmeyer. 2019. Protein phosphatase 2A as a therapeutic target in inflammation and neurodegeneration. *Pharmacol. Ther.* 201: 181–201.
75. Sager, R. A., M. R. Woodford, S. J. Backe, A. M. Makedon, A. J. Baker-Williams, B. T. DiGregorio, D. R. Loiselle, T. A. Haystead, N. E. Zachara, C. Prodromou, et al. 2019. Post-translational regulation of FNIP1 creates a rheostat for the molecular chaperone Hsp90. *Cell Rep.* 26: 1344–1356.e5.
76. Yang, F. M., H. M. Chang, and E. T. H. Yeh. 2021. Regulation of TLR4 signaling through the TRAF6/sNASP axis by reversible phosphorylation mediated by CK2 and PP4. *Proc. Natl. Acad. Sci. USA* 118: e2107044118.
77. Verlee, A., S. Mincke, and C. V. Stevens. 2017. Recent developments in antibacterial and antifungal chitosan and its derivatives. *Carbohydr. Polym.* 164: 268–283.
78. Zhou, H. X., and X. Pang. 2018. Electrostatic interactions in protein structure, folding, binding, and condensation. *Chem. Rev.* 118: 1691–1741.
79. Csanády, L., P. Vergani, and D. C. Gadsby. 2019. Structure, gating, and regulation of the CFTR anion channel. *Physiol. Rev.* 99: 707–738.
80. Li, Z., J. Zhao, I. Tikhanovich, S. Kuravi, J. Helzberg, K. Dorko, B. Roberts, S. Kumer, and S. A. Weinman. 2016. Serine 574 phosphorylation alters transcriptional programming of FOXO3 by selectively enhancing apoptotic gene expression. *Cell Death Differ.* 23: 583–595.
81. Long, L., Y. Deng, F. Yao, D. Guan, Y. Feng, H. Jiang, X. Li, P. Hu, X. Lu, H. Wang, et al. 2014. Recruitment of phosphatase PP2A by RACK1 adaptor protein deactivates transcription factor IRF3 and limits type I interferon signaling. *Immunity* 40: 515–529.
82. White, T. E., A. Brandariz-Nuñez, J. C. Valle-Casuso, S. Amie, L. A. Nguyen, B. Kim, M. Tuzova, and F. Diaz-Griffero. 2013. The retroviral restriction ability of SAMHD1, but not its deoxynucleotide triphosphohydrolase activity, is regulated by phosphorylation. *Cell Host Microbe* 13: 441–451.
83. Schott, K., N. V. Fuchs, R. Derua, B. Mahboubi, E. Schnellbächer, J. Seifried, C. Tondera, H. Schmitz, C. Shepard, A. Brandariz-Nuñez, et al. 2018. Dephosphorylation of the HIV-1 restriction factor SAMHD1 is mediated by PP2A-B55α holoenzymes during mitotic exit. *Nat. Commun.* 9: 2227.
84. Wang, C., L. Ruan, H. Shi, W. Lin, L. Liu, and S. Li. 2021. Phosphorylation of shrimp Tcf by a viral protein kinase WSV083 suppresses its antiviral effect. *Front. Immunol.* 12: 698697.
85. Gielens, C., N. De Geest, F. Compernolle, and G. Préaux. 2004. Glycosylation sites of hemocyanins of *Helix pomatia* and *Sepia officinalis*. *Micron* 35: 99–100.